



# The diurnal variability of atmospheric nitrogen oxides (NO and NO<sub>2</sub>) above the Antarctic Plateau driven by atmospheric stability and snow emissions

M. M. Frey<sup>1</sup>, N. Brough<sup>1</sup>, J. L. France<sup>2</sup>, P. S. Anderson<sup>1,3</sup>, O. Traulle<sup>4</sup>, M. D. King<sup>2</sup>, A. E. Jones<sup>1</sup>, E. W. Wolff<sup>1</sup>, and J. Savarino<sup>5</sup>

<sup>1</sup>British Antarctic Survey, Natural Environment Research Council, Cambridge, UK

<sup>2</sup>Department of Earth Sciences, Royal Holloway, University of London, Egham, UK

<sup>3</sup>Scottish Association for Marine Science, Oban, Argyll, Scotland, PA37 1QA, UK

<sup>4</sup>CNRM-GAME, URA 1357, Météo France CNRS, Toulouse, France

<sup>5</sup>Université Joseph Fourier – Grenoble 1/CNRS-INSU, Laboratoire de Glaciologie et Géophysique de l'Environnement, St. Martin d'Hères, France

Correspondence to: M. M. Frey (maey@bas.ac.uk)

Received: 31 July 2012 – Published in Atmos. Chem. Phys. Discuss.: 29 August 2012

Revised: 1 February 2013 – Accepted: 28 February 2013 – Published: 15 March 2013

**Abstract.** Atmospheric nitrogen oxides (NO and NO<sub>2</sub>) were observed at Dome C, East Antarctica (75.1° S, 123.3° E, 3233 m), for a total of 50 days, from 10 December 2009 to 28 January 2010. Average ( $\pm 1\sigma$ ) mixing ratios at 1.0 m of NO and NO<sub>2</sub>, the latter measured for the first time on the East Antarctic Plateau, were 111 ( $\pm 89$ ) and 98 ( $\pm 89$ ) pptv, respectively. Atmospheric mixing ratios are on average comparable to those observed previously at South Pole, but in contrast show strong diurnal variability: a minimum around local noon and a maximum in the early evening coincide with the development and collapse of a convective boundary layer. The asymmetric diurnal cycle of NO<sub>x</sub> concentrations and likely any other chemical tracer with a photolytic surface source is driven by the turbulent diffusivity and height of the atmospheric boundary layer, with the former controlling the magnitude of the vertical flux and the latter the size of the volume into which snow emissions are transported. In particular, the average ( $\pm 1\sigma$ ) NO<sub>x</sub> emission flux from 22 December 2009 to 28 January 2010, estimated from atmospheric concentration gradients, was  $8.2 (\pm 7.4) \times 10^{12}$  molecule m<sup>-2</sup> s<sup>-1</sup> belongs to the largest values measured so far in the polar regions and explains the 3-fold increase in mixing ratios in the early evening when the boundary layer becomes very shallow. Dome C is likely not representative for the entire East Antarctic Plateau but il-

lustrates the need of an accurate description of the boundary layer above snow in atmospheric chemistry models. A simple nitrate photolysis model matches the observed median diurnal NO<sub>x</sub> flux during the day but has significant low bias during the night. The difference is significant taking into account the total random error in flux observations and model uncertainties due to the variability of NO<sub>3</sub><sup>-</sup> concentrations in snow and potential contributions from NO<sub>2</sub><sup>-</sup> photolysis. This highlights uncertainties in the parameterization of the photolytic NO<sub>x</sub> source in natural snowpacks, such as the poorly constrained quantum yield of nitrate photolysis. A steady-state analysis of the NO<sub>2</sub> : NO ratios indicates that peroxy (HO<sub>2</sub> + RO<sub>2</sub>) or other radical concentrations in the boundary layer of Dome C are either higher than measured elsewhere in the polar regions or other processes leading to enhanced NO<sub>2</sub> have to be invoked. These results confirm the existence of a strongly oxidising canopy enveloping the East Antarctic Plateau in summer.

## 1 Introduction

The nitrogen oxides NO and NO<sub>2</sub> (NO + NO<sub>2</sub> = NO<sub>x</sub>) play a key role in determining the oxidizing capacity of the atmospheric boundary layer in the high latitudes. This influence

is achieved via photolysis of  $\text{NO}_2$ , the only source for in situ production of tropospheric ozone ( $\text{O}_3$ ), through shifting  $\text{HO}_x$  radical partitioning towards the hydroxyl radical (OH) via the reaction  $\text{NO} + \text{HO}_2 \rightarrow \text{NO}_2 + \text{OH}$ , and finally through reactions with peroxyradicals  $\text{NO} + \text{HO}_2$  (or  $\text{RO}_2$ ) also controlling formation rates of peroxides ( $\text{H}_2\text{O}_2$  and  $\text{ROOH}$ ). Atmospheric  $\text{NO}_x$  concentrations in coastal Antarctica are small, with build up in part prevented by gas-phase formation of halogen nitrates (e.g.  $\text{BrNO}_3$ ,  $\text{INO}_3$ ) followed by their heterogeneous loss (Grannas et al., 2007; Bauguitte et al., 2012), whereas mixing ratios reported from South Pole are unusually high equaling those from the mid-latitudes (Davis et al., 2008). Large mixing ratios of  $\text{NO}_x$  are, in part, due to significant emissions from surface snow observed at various polar sites, equal or exceeding in magnitude their gas phase source (Grannas et al., 2007; Jones et al., 2011, and refs. therein), and are attributed to UV-photolysis of nitrate in snow (Grannas et al., 2007; Frey et al., 2009b). Significant changes of atmospheric oxidising capacity due to emissions of  $\text{NO}_x$  from snow occur above snow covered areas. For example, net ozone production was observed in the interior of Antarctica (Crawford et al., 2001; Legrand et al., 2009; Slusher et al., 2010) and unusually high levels of hydroxyl radical levels were detected at South Pole (Davis et al., 2008, and refs. therein). Furthermore, release of NO from snow is associated with the inter-seasonal variability of hydrogen peroxide ( $\text{H}_2\text{O}_2$ ) above polar snow, since the reaction  $\text{HO}_2 + \text{NO}$  competes with the recombination reaction  $\text{HO}_2 + \text{HO}_2 \rightarrow \text{H}_2\text{O}_2$  (e.g. Frey et al., 2005, 2009a).

Here we recall the basic gas phase chemistry of  $\text{NO}_x$  as described by the Leighton mechanism (Leighton, 1961):



The conversion of NO back to  $\text{NO}_2$  via Reaction (R3) proceeds through additional channels when other oxidants are present, such as hydroxyl (OH), peroxy ( $\text{RO}_2$ ) or halogen (XO, with X=Cl, Br, I) radicals:



$\text{NO}_2$  reacts further with hydroxyl or halogen radicals to form  $\text{HNO}_3$  or  $\text{XNO}_3$  which is then deposited to the snow surface:



Reaction rate constants can be found for example in Sander and Bottenheim (2012). The following simplified reaction scheme summarises the main channels of  $\text{NO}_x$  production from  $\text{NO}_3^-$  photolysis taking place inside and on the

surface of snow grains (Grannas et al., 2007):



For example, photolysis rate constants of  $\text{NO}_3^-$  (Reaction R10) were experimentally determined for the East Antarctic snow pack as a function of solar zenith angle and snow depth (France et al., 2011). Major atmospheric chemistry campaigns such as ISCAT and ANTICI at South Pole and CHABLIS at Halley provided the first extensive observations of composition and oxidising capacity of the lower troposphere above Antarctica, including observations of  $\text{NO}_x$  (Davis et al., 2004b; Eisele et al., 2008; Jones et al., 2008). There is now consensus that  $\text{NO}_x$  emissions are an essential component of air-snow cycling of oxidised nitrogen species above the polar ice sheets and snow-covered surfaces in the mid-latitudes (Honrath et al., 2000; Grannas et al., 2007; Davis et al., 2008; Frey et al., 2009b). However, the quantitative understanding of  $\text{NO}_x$  emissions from snow is still incomplete and parameterizations for use in global chemistry-climate models are either non-existent or not reflecting recent progress from lab and field studies (Bartels-Rausch et al., 2012).

The study presented here is motivated by the sparse data base of  $\text{NO}_2$  observations above snow and a general lack of comparable measurements of  $\text{NO}_x$  emissions from surface snow across a wide range of environmental conditions. Reported for the first time are observations of both nitrogen oxides in air above the plateau region of the East Antarctic Ice Sheet and their flux estimated from the measurement of concentration gradients. The observed diurnal variabilities of  $\text{NO}_x$  concentrations are discussed with respect to mixing properties of the atmospheric boundary layer and strength of the snow pack source. Measured  $\text{NO}_x$  flux is compared to model predictions to diagnose uncertainties in the parameterization of the  $\text{NO}_x$  source in surface snow. And finally, atmospheric  $\text{NO}_2$  :  $\text{NO}$  ratios are used to infer potential radical concentrations.

## 2 Methods

Measurements of atmospheric  $\text{NO}_x$  for a total of 50 days, from 10 December 2009 to 28 January 2010, took place at Dome C, where the year-round operated French-Italian Concordia Station is located (75.1° S, 123.3° E, 3233 m). The local climate is dominated by temperature inversion or katabatic winds that coincide with cold, clear and calm conditions. However, wind speeds are low in comparison to near-coastal areas due to the location on top of a Dome, where surface slopes do not exceed 1%. Occasional synoptic coastal

influence coincides with higher wind speeds and brings relatively warmer and cloudier air to the site (e.g. Genthon et al., 2010).

Atmospheric sampling was done out of an electrically heated lab shelter (Weatherhaven tent) located in the designated clean-air sector 0.7 km upwind (South) of Concordia station (Fig. 1a). Apart from snow drift due to the shelter structure the surrounding snow pack had not been subject to any perturbations such as motorized vehicle or foot traffic for the past 4–5 yr.

Ancillary data collected were standard meteorology from an automatic weather station (AWS) at 0.5 km distance (Fig. 1a), including air temperature (Vaisala PT100 DTS12 at 1.6 m), relative humidity at 1.6 m, wind speed and direction (Vaisala WAA 15A at 3.3 m), as well as *in situ* measurements of temperature of air (PT100 class 1/10 mounted in a passively ventilated radiation shield at 1 m) and of the snow surface (Campbell Scientific infrared radiometer IRR-P), and broadband UV-A irradiance (Kipp & Zonen UVA CUV4 at 1 m). Measurements of the three-dimensional wind components ( $u$ ,  $v$ ,  $w$ ) and temperature at 10 Hz by a sonic anemometer (ATEC1-061101 at 7 m) mounted on a tower at 1.2 km distance were used to derive atmospheric turbulence parameters (Fig. 1a). Observations of ozone mixing ratios (Thermo Electron Corporation model 49I, Franklin, Massachusetts) at 15 m from Concordia station were also available (Legrand et al., 2009). Note that all times are given as local time (LT), equivalent to UTC + 8 h, and that during the study period the sun never set below the horizon.

## 2.1 NO<sub>x</sub> detection

For NO<sub>x</sub> detection a 2-channel chemiluminescence detector (CLD) was used that was run previously year-round at Halley (75.6° S, 26.6° W, 37 m) in coastal Antarctica (Bauguitte et al., 2012). The detection technique is based on the reaction of NO with excess O<sub>3</sub> (Reaction R3) to produce electronically excited NO<sub>2</sub> followed by the measurement of photons emitted by NO<sub>2</sub> returning to the ground state. One channel of the CLD measured atmospheric NO whereas the other determined the sum of NO and NO originating from the quantitative photolytic conversion of NO<sub>2</sub> (Reaction R1) (Fig. 1b). The signal difference between the two channels was then used to calculate atmospheric NO<sub>2</sub> concentrations. Three 20 m-long intake lines (Fluoroline 4200 high purity PFA, I.D. 4.0 mm) were mounted on a mast about 15 m upwind outside the snow drift zone surrounding the lab shelter to sample air at 0.01, 1.00 and 4.00 m above the natural snow pack. During selected time periods firm air (interstitial air) was sampled by inserting one inlet into pre-cored horizontal holes at 5–10 cm snow depth.

The sample intakes were shielded from solar radiation with black heat-shrink tubing and connected inside the lab shelter to a valve box, which automatically switched the CLD between sampling heights on a 90 s duty cycle (Fig. 1b).

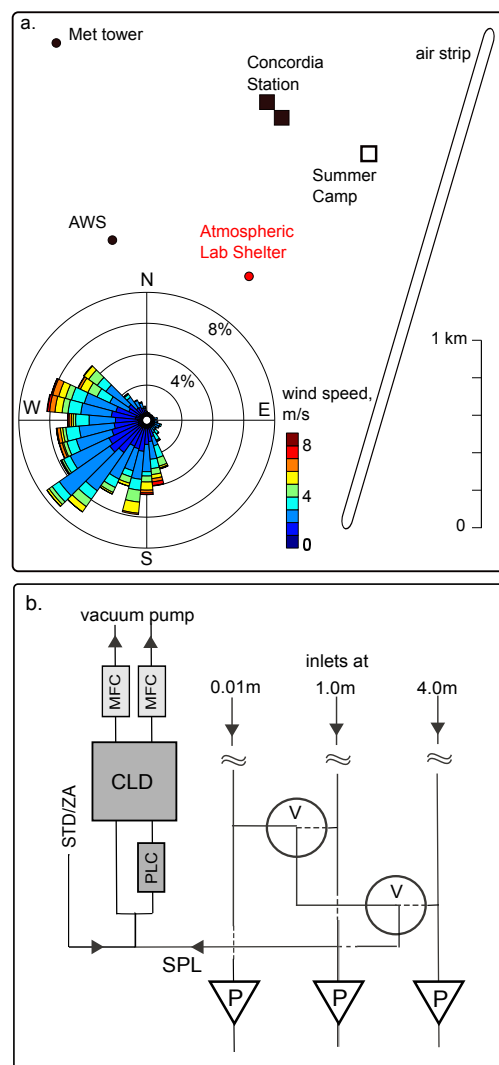


**Fig. 1.** (a) The wind rose for Dome C during December 2009 to January 2010 and location map of the atmospheric lab shelter, air strip, Concordia station, automatic weather station (AWS) and meteorology tower with sonic anemometer. (b) Schematic of the NO<sub>x</sub> sampling set up: sample air (SPL) is drawn continuously by vacuum pumps (P) from 3 inlet heights which are sampled by automatic switching of two 3-way valves (V). Sample flow into the chemiluminescence detector (CLD) through two channels, one with photolytic converter (PLC), is regulated by mass flow controllers (MFC). For calibration NO gas standard (STD) and for artefact tests zero air (ZA) are added upstream of the PLC. Triangles indicate flow direction (details in text).

In order to achieve continuous flow and reduce sample residence time in the tubing, ambient air was drawn through each one of the long intake lines at 5.0 STP-Lmin<sup>-1</sup> using high-capacity vacuum diaphragm pumps (GAST, Part No. DOA-P725-BN) (Fig. 1b). The CLD inlet drawing sample air from the respective intake line was mass-flow controlled at 1.0 STP-Lmin<sup>-1</sup> for each channel (Fig. 1b). Spike tests

**Table 1.** Overview of parameters characterizing CLD instrument performance at Dome C.

Parameter	NO	NO <sub>2</sub>	Number of samples
NO sensitivity <sup>a</sup> , Hz pptv <sup>-1</sup>	4.5 (4.4–4.7)	2.5 (2.1–3.0)	23 (CLD1)/35 (CLD2)
artefact <sup>b</sup>	37 Hz (8–9 pptv)	8 Hz (8–11) pptv	29
CE <sup>c</sup>	–	0.30 (0.25–0.35)	64
random error <sup>d</sup> , pptv	1.5 (1.3)	11.1 (9.6)	all data
precision <sup>e</sup> , %	2.6 (1.6)	97.8 (15.2)	all data
HONO interference <sup>f</sup>	–	0.22	–

<sup>a</sup> mean (range);<sup>b</sup> mean (range) during 11 December 2009–3 January 2010, after that about half that value, but not used for correction (see text). The range is based on the observed variability in sensitivity;<sup>c</sup> mean (range) of photolytic conversion efficiency CE for NO<sub>2</sub>;<sup>d</sup> mean (median) 1- $\sigma$  standard error of the 1-min averages;<sup>e</sup> mean (median) relative 1- $\sigma$  standard error from the 1-min averages;<sup>f</sup> maximum theoretical interference of HONO in the NO<sub>2</sub> signal (see text).

using the NO gas standard showed that air sample residence time between the tip of the sample intake and the reaction vessel inside the CLD was 4 s, and therefore < 2 s in the photolytic cell. On three occasions ambient air was sampled for up to 1.5 h through all three inlets mounted at 1.00 m above the snow. Parametric (two-sample *t* test) and non-parametric tests (Wilcoxon signed rank test) performed on NO and NO<sub>2</sub> mixing ratios did not show any significant differences between the inlets at the 95 % confidence level.

Transforming CLD count rates into atmospheric mixing ratios required regular measurement of baseline, instrument sensitivity, detector artefacts and conversion efficiency (CE) of Reaction (R1) taking place in the photolytic converter (Table 1). Baseline count rates were determined by adding excess ozone to sample air in a pre-chamber so that all electronically excited NO<sub>2</sub> has returned to ground state when reaching the reaction chamber. The baseline was measured for 60 s every 13.5 min alternating between all three inlets. The NO sensitivity of the CLDs was determined every 14 h by standard addition to the sample air matrix of a 1 ppmv NO/NO<sub>2</sub> mixture (UK National Physical Laboratory traceable BOC certified), which is further diluted to 4 ppbv of NO. Some of the automated calibrations were compromised by a small leak and the respective CLD sensitivities were then replaced by average values confirmed by pre- and post-season calibrations. CE was determined by addition of a known mole-fraction of NO<sub>2</sub>. This was achieved by gas phase titration of the NO/NO<sub>2</sub> mixture to NO<sub>2</sub> by O<sub>3</sub> generated from a pen-ray Hg lamp, and monitoring the un-titrated NO mole fraction. The instrument artefact originating from NO<sub>x</sub> producing surface reactions in inlets and reaction cells was determined by overflowing the instrument inlet with scrubbed ambient air supplied by a pure air generator (Eco-Physics PAG003) (Fig. 1b). The artefact was measured every 14 h, offset by 7 h to the calibration runs.

## 2.2 NO<sub>x</sub> data processing and uncertainty

The averaged baseline intervals were linearly interpolated and then subtracted from the CLD count rates recorded at 1 Hz. The baseline levels were typically the same in between the three inlets, but showed large and systematic variations when NO<sub>x</sub> concentrations between the three inlets were very different, i.e. when either near-surface gradients were pronounced during certain times of the day or when firn air was sampled. During these sampling periods the signals from each inlet were corrected individually by subtracting only the baseline interval corresponding to the specific inlet. The repeat period of baseline measurement for the individual inlet increased therefore from 13.5 to 40.5 min. An artefact correction was applied during the 11 December 2009 to 3 January 2010 period, amounting to 8–9 pptv and 8–11 pptv for NO and NO<sub>2</sub>, respectively (Table 1). After 4 January 2010 artefact levels dropped to about 50 % of the above values and were not used.

CE was on average 0.30 (range 0.25–0.35) (Table 1), thus considerably lower than a CE of 0.55–0.60 reported for the same instrument operated at sea level (Bauguitte et al., 2012). We explain this as follows: if one neglects oxidants in ambient air CE depends solely on the photolysis rate *j* and sample residence time  $\tau$  in the photolytic cell of the CLD (Ryerson et al., 2000):

$$CE = 1 - e^{-j\tau} \quad (1)$$

The former is a function of the optical geometry of the instrument, which had remained unchanged, whereas the latter decreases with altitude since the photolytic cell was not pressure controlled. Mean ambient pressure (652 mbar) and temperature (242 K) at Dome C result in a volumetric flow rate about 0.72 that at Halley. Inserting into Eq. (1) the respective values for Dome C (DC) and Halley and taking the ratio yields.

$$\frac{\tau_{DC}}{\tau_{Halley}} = \frac{\ln(1 - CE_{DC})}{\ln(1 - CE_{Halley})} \quad (2)$$

With  $CE_{\text{Halley}}$  of 0.55 and a ratio of  $\tau_{\text{DC}}/\tau_{\text{Halley}}$  of 0.72 one obtains a  $CE_{\text{DC}}$  of 0.44. Contrary to Halley long sample intake lines were used continuously at Dome C causing a pressure drop inside the photolytic cell of  $\sim 110$  mb estimated from flow rates, temperature and inlet diameter. This further reduces the theoretical  $CE_{\text{DC}}$  to 0.38. Thus most of the difference in CE can be attributed to lower pressure and thus a shorter residence time of sample air in the photolytic cell.

Shielding an air sample from solar radiation once entering the sample line can potentially alter the ratio of  $\text{NO}_2$  and  $\text{NO}$  as the Leighton photostationary state (R1–R3) shifts to a new equilibrium. Formation of  $\text{NO}_2$  from Reaction R3 at Dome C during this study was estimated to be  $4 \times 10^6$  molecule  $\text{cm}^{-3} \text{s}^{-1}$ . With a sample residence time in the inlets of  $< 4$  s one obtains median changes in  $\text{NO}$  and  $\text{NO}_2$  of  $< 1.6\%$  and therefore no correction was applied.

The mean wind direction during the field campaign was from SSW ( $208^\circ$ ) with an average speed of  $2.6 \text{ ms}^{-1}$  (Fig. 1a). During less than 1 % of measurement time the wind came from Concordia station carrying polluted air from the station power generator to the measurement site (Fig. 1a). To remove pollution spikes a moving 1-min standard deviation filter was applied rejecting data when  $1-\sigma$  of  $\text{NO}$  and  $\text{NO}_2$  mixing ratios within the 1-min window exceeded 24 and 90 pptv, respectively. Comparison to logged contamination events and the above wind rose analysis confirmed the efficiency of the statistical filter in suppressing any pollution episode either from power generators at Concordia station or occasional vehicle traffic (air planes, snowmobiles).

Filtered data were then aggregated to 1 min averages. About 6.3 % of the  $\text{NO}_2$  mixing ratios, equivalent to 65 h, are negative due to uncertainties in baseline and artefact determinations, but are included in the final dataset to avoid statistical bias. The uncertainty in the 1-min averages due to random errors was estimated as the  $1-\sigma$  standard error  $\bar{\sigma} = \sigma/\sqrt{N}$ , with standard deviation  $\sigma$  and number of samples  $N$ . The average  $\bar{\sigma}$  was 1.5 and 11.1 pptv for  $\text{NO}$  and  $\text{NO}_2$ , respectively (Table 1). Average precision calculated as the mean relative  $1-\sigma$  standard error from the 1-min averages was 2.6 and 97.8 % for  $\text{NO}$  and  $\text{NO}_2$ , respectively (Table 1). Taking the median precision yields 1.6 and 15.2 % for  $\text{NO}$  and  $\text{NO}_2$ , respectively (Table 1). Errors in  $\text{NO}_2$  measurements are thus larger than seen at Halley (Bauguitte et al., 2012) mostly due to the reduced conversion efficiency at Dome C.

Quantification of  $\text{NO}_2$  as  $\text{NO}$  after photolytic conversion can be compromised by the presence of other chemical gas phase species, which produce  $\text{NO}$  in the photolytic converter, i.e. whose absorption cross sections have significant overlap with that of  $\text{NO}_2$  (Fig. 2b). During polar day these are bromine nitrate ( $\text{BrONO}_2$ ) and nitrous acid ( $\text{HONO}$ ) (Ryerson et al., 2000), of which only the latter its expected to play a role on the East Antarctic Plateau. We therefore calculated a potential interference as the ratio of the respective photolysis rate constants,  $j_{\text{HONO}}/j_{\text{NO}_2}$ , in the photolytic converter (Fig. 2) and obtained a value of 0.22, somewhat smaller than

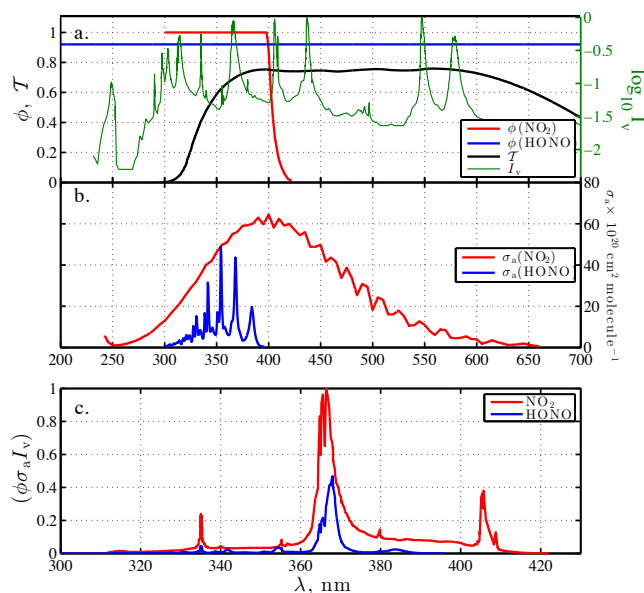


**Fig. 2.** The potential interference of HONO in the detection of  $\text{NO}_2$  was estimated using (a) the scaled intensity  $I_v$  of the photolytic converter (200-W high pressure arc mercury lamp, USHIO-200DP), the respective quantum yield  $\phi$ , total transmittance  $\mathcal{T}$  of the optical filters, including a Pyrex window (Oriel, Part No. 60127) and a KBr filter (KG3, Oriel Part No. 51960), (b) the respective absorption cross sections  $\sigma_a$  (Sander et al., 2006) and (c) scaled  $(\phi\sigma_a I_v)$  in order to calculate respective photolysis rate constants  $j = \int \phi\sigma_a I_v d\lambda$  and their ratio.  $\lambda$  is wavelength and note different scale of x-axis in (c).

that of 0.37 estimated for a similar instrument (Ryerson et al., 2000). Median HONO mixing ratios from laser-induced fluorescence at South Pole in Summer were 5.8 pptv (maximum 18.2 pptv) (Liao et al., 2006) and would imply that the seasonal average  $\text{NO}_2$  at 1 m was overestimated by 1.3 % (maximum 4.3 %). Mean HONO mixing ratios measured with a wet chemical method at Dome C during December 2010 and January 2011 were 28 pptv and showed diurnal variability with morning (06:00 LT) and evening (21:00 LT) maxima (Kerbrat et al., 2012). A potential interference from  $\text{HNO}_4$  was stated to be small (Kerbrat et al., 2012). If HONO mixing ratios were similar at Dome C in summer 2009–10, then the seasonal mean of  $\text{NO}_2$  at 1.0 m of 98 pptv (Table 2) would be overestimated by 6.7 %. The overestimate could be up to  $\sim 13\%$  from morning to noon if the median diurnal cycles of  $\text{NO}_2$  and HONO are taken into account. As no HONO measurements were available, we did not apply any correction to the  $\text{NO}_2$  data.

### 2.3 $\text{NO}_x$ flux estimates

$\text{NO}_x$  flux was derived based on the integrated flux gradient method (e.g. Lenschow, 1995) and using  $\text{NO}_x$  mixing ratios measured at 0.01 and 1.0 m. Fick's Law describes how concentration gradient  $\partial c/\partial z$  and diffusion coefficient  $K_c$  of a

**Table 2.** NO<sub>x</sub> mixing ratios and flux at Dome C during 22 December 2009–28 January 2010.

Parameter	<i>z</i> , m	mean ± 1σ	median	maximum	<i>t</i> <sub>total</sub> , days <sup>a</sup>
NO, pptv	1.0 <sup>b</sup>	111 ± 89	84	565	23.2
	firn	226 ± 217	150	3043	3.7
	0.01	117 ± 93	90	774	12.6
	1.0	102 ± 79	82	565	13.6
	4.0	85 ± 48	77	298	7.7
NO <sub>2</sub> , pptv	1.0 <sup>b</sup>	98 ± 89	71	616	21.8
	firn	345 ± 277	243	3051	3.7
	0.01	96 ± 76	73	477	12.4
	1.0	74 ± 70	53	616	13.2
	4.0	59 ± 56	46	463	7.6
NO <sub>x</sub> , pptv	1.0 <sup>b</sup>	206 ± 155	157	942	21.7
	firn	572 ± 470	386	5247	3.7
	0.01	210 ± 153	165	1001	12.3
	1.0	175 ± 135	137	860	13.2
	4.0	144 ± 92	124	630	7.6
NO <sub>2</sub> : NO	1.0 <sup>b</sup>	1.1 ± 1.7	0.8	87	21.7
	firn	1.9 ± 1.1	1.5	18.5	3.7
	0.01	1.0 ± 0.9	0.8	17.4	12.3
	1.0	0.9 ± 1.2	0.6	83	13.2
	4.0	0.8 ± 2.0	0.6	40	7.6
F–NO <sub>x</sub> × 10 <sup>12</sup> molecule m <sup>-2</sup> s <sup>-1</sup>	0.01–1.0	8.2 ± 7.4	6.8	73.6	7.1
F–NO <sub>x</sub> × 10 <sup>12</sup> molecule m <sup>-2</sup> s <sup>-1</sup> , local noon	0.01–1.0	9.4 ± 9.0	9.1	32.2	0.4
F–NO <sub>x</sub> × 10 <sup>12</sup> molecule m <sup>-2</sup> s <sup>-1</sup> , local midnight	0.01–1.0	7.7 ± 7.1	4.8	27.1	0.2

<sup>a</sup> Total sample time estimated as the sum of all 1-min intervals;<sup>b</sup> 10 December 2009 to 28 January 2010.

chemical tracer relate to its diffusive flux  $F$ .

$$F = -K_c \frac{\partial c}{\partial z} \quad (3)$$

Within the atmospheric boundary layer, vertical transport is dominated by turbulence, rather than molecular diffusion, and  $K_c$  can be estimated by direct measurements of the turbulent diffusivity for momentum  $K_m$  and heat  $K_h$ . In this study, sonic anemometer measurements of atmospheric turbulence were used from a tower at 1.2 km distance, since *in situ* observations were compromised due to instrument malfunctioning (Fig. 1a). Turbulence measurements not collocated with NO<sub>x</sub> observations are expected to be less problematic at Dome C as the fetch is highly homogeneous, but estimated uncertainties are included in the total flux uncertainty described below.  $K$  values are calculated according to the Monin-Obukhov similarity theory (MOST) whose predictions of flux-profile relationships at Halley, an Antarctic coastal site of the same latitude as DC, agree well with observations (Anderson and Neff, 2008, and references therein). For the chemical flux estimate we make the assumption that  $K_c \sim K_h$ . The NO<sub>x</sub> flux  $F$  is then given by

$$F = -\frac{\kappa u_* z}{\Phi_h(\frac{z}{L})} \frac{\partial c}{\partial z} \quad (4)$$

where  $\kappa$  (set to 0.40) is the von Karman constant,  $u_*$  is the friction velocity,  $z$  is height, and  $\Phi_h(\frac{z}{L})$  an empirically determined stability function for heat with  $L$  as the Monin-Obukhov length. Assuming constant flux across the layer between the two measurement heights  $z_1$  and  $z_2$  allows to integrate and yields:

$$F = -\frac{\int_{c_1}^{c_2} \kappa u_* \partial c}{\int_{z_1}^{z_2} \Phi_h(\frac{z}{L}) \frac{\partial z}{z}} = -\frac{\kappa u_* [c(z_2) - c(z_1)]}{\int_{z_1}^{z_2} \Phi_h(\frac{z}{L}) \frac{\partial z}{z}} \quad (5)$$

Stability functions used were  $\Phi_h = \text{Pr}_t + 4.62z/L$  established previously for stable conditions above snow (King and Anderson, 1994) and  $\Phi_h = \text{Pr}_t(1 - 11.6z/L)^{-0.5}$  for unstable conditions (Hoegstroem, 1988), where the Prandtl number  $\text{Pr}_t$  is set to 0.95. Integrated forms of  $\Phi_h$  can be found in Jacobson (1999). Note that in the neutral boundary layer  $\Phi_h = \text{Pr}_t$  and the denominator in Eq. (5) simplifies to  $\text{Pr}_t \ln(z_2/z_1)$ . Friction velocity  $u_*$  and  $L$  were computed from the three-dimensional wind components ( $u$ ,  $v$ ,  $w$ ) and temperature measured by the sonic anemometer. The instrument alternated between 10 min of measurements and 10 min of heating to prevent frost build up on the sensors. Processing in 10-min blocks included despiking, temperature cross-wind correction and a double coordinate rotation to force mean  $w$

to zero (Kaimal and Finnigan, 1994; Van Dijk et al., 2006). Eq. (5) implies that a positive flux is in upward direction, equivalent to snow pack emissions and a negative flux is in downward direction, equivalent to deposition.

The application of MOST requires that (a) flux is constant between measurement heights  $z_1$  and  $z_2$ , (b) the lower inlet height  $z_1$  is well above the aerodynamic roughness length of the surface, (c) the upper inlet height  $z_2$  is within the surface layer, i.e. below 10 % of the boundary layer height  $h_z$  (Stull, 1988), and (d)  $z_1$  and  $z_2$  are far enough apart to allow for detection of a significant concentration difference [ $c(z_2) - c(z_1)$ ]. Calculated flux values are filtered based on these criteria as described below.

For (a) the chemical lifetime ( $\tau_{\text{chem}}$ ) needs to be much longer than the turbulent transport time scale ( $\tau_{\text{trans}}$ ) of the chemical tracer. A typical  $\tau_{\text{trans}}$  is calculated as the product of layer thickness, i.e. distance between the surface roughness length for heat ( $z_{0,h}$ ) and reference height  $z_r$  (here the upper inlet height of 1 m), and aerodynamic resistance  $R_a$ .

$$\tau_{\text{trans}} = (z_r - z_{0,h})R_a \quad (6)$$

$R_a$  of a gas is estimated from similarity theory as the inverse of the turbulent diffusivity for heat  $K_h = \frac{\kappa u_* z}{\Phi_h(\frac{z}{L})}$  (Eq. 4) integrated over the layer thickness (Jacobson, 1999):

$$\tau_{\text{trans}} = (z_r - z_{0,h}) \int_{z_{0,h}}^{z_r} \frac{\partial z}{K_h} = (z_r - z_{0,h}) \frac{\int_{z_{0,h}}^{z_r} \Phi_h(\frac{z}{L}) \frac{\partial z}{z}}{\kappa u_*} \quad (7)$$

During the study period  $\tau_{\text{trans}}$  was on average on the order of  $\sim 10$  min assuming  $z_{0,h}$  is similar to the surface roughness length of momentum  $z_{0,m}$  measured at Halley (King and Anderson, 1994).  $\tau_{\text{chem}}$  of NO and NO<sub>2</sub> is short due to rapid interconversion on the order of seconds. However, previous estimates of  $\tau_{\text{chem}}$  for NO<sub>x</sub> range between 6.4 h (daily mean) at Halley (Bauguitte et al., 2012) and 8 h (median) at South Pole (Davis et al., 2004a). With  $\tau_{\text{chem}}$  of NO<sub>x</sub> exceeding  $\tau_{\text{trans}}$  by a factor  $\sim 40$  it can be assumed that the flux of nitrogen oxides  $F_{\text{NO}_x}$  between measurement heights is approximately constant.

For (b) it is assumed that snow properties at Dome C are similar to those at Halley, being compacted, sintered firn with some sastrugi and a  $z_{0,m}$  value of  $(5.6 \pm 0.6) \times 10^{-5}$  m (King and Anderson, 1994). A lower inlet at 0.01 m is therefore many scale lengths above this length. There is an unknown element of inlet capture, in that in perfectly calm wind conditions, air is drawn in from both above and below this height. This may have a biased effect due to the theoretical curvature of the concentration and indeed such bias may even exist during turbulence (assumed to be ubiquitous at this height at Dome C). Such bias is small, however: typical  $2 \text{ m s}^{-1}$  winds at 4 m imply a  $1 \text{ m s}^{-1}$  wind at 0.01 m. Sample flow rate of  $5.0 \text{ STP-L min}^{-1}$  at this speed gives a radius scale of 0.9 mm: that is, the air sample is an average of a disc of radius 0.9 mm around the sample level of 10 mm. The mean concentration

$c$  has curvature due to the gradient being to a first approximation proportional to  $1/z$ . Hence the concentration changes proportionally to  $\ln(z)$ . The relative difference between a sample at exactly 10 mm and an average of 9 and 11 mm is therefore the difference between  $(\ln(0.011) + \ln(0.009))/2$  and  $\ln(0.01)$  or  $< 0.2\%$ .

For (c) the upper inlet height of 1 m is compared to estimates of mixing height  $h_z$  using parameterizations after Pollard et al. (1973) and Zilitinkevitch et al. (2002) described previously for analysis of boundary layer behaviour at South Pole (Neff et al., 2008). Since diurnal cycles are present at Dome C the use of these simple scaling laws warrants caution as they apply to the stable or weakly unstable boundary layer and assume that an equilibrium boundary layer depth is reached. Nevertheless, the parameterization after Pollard et al. (1973) compared well with observed profiles at Summit, Greenland (Cohen et al., 2007), a site of similar diurnal radiative forcing at the top of the atmosphere, and at South Pole during very stable conditions with  $h_z < 50$  m (Neff et al., 2008). Therefore at Dome C  $h_z$  was calculated only for the stable boundary layer, i.e. in the case of Pollard et al. (1973) only when the vertical gradient of potential temperature was positive and for Zilitinkevitch et al. (2002) only when Monin-Obukhov length  $L > 0$ . NO<sub>x</sub> flux values were filtered when at least one parameterisation predicted  $h_z < 10$  m resulting in the removal of 23.0 % (369 values) of all available 10-min flux averages.

For (d) 10-min averages of [ $c(z_2) - c(z_1)$ ] not significantly different from zero, i.e. smaller than their respective  $1-\sigma$  standard error, were not included in the NO<sub>x</sub> flux estimates. The  $1-\sigma$  standard error in [ $c(z_2) - c(z_1)$ ] was determined by error propagation of the  $1-\sigma$  standard error of NO<sub>x</sub> mixing ratios. A total of 13.1 % (210 values) of all available 10-min flux averages were removed. It should be noted that choosing to sample close to the surface does significantly enhance the signal in  $c$ , e.g. the signal between 1.00 m and 0.01 m is double that between 1.00 m and 0.10 m, whilst between 4 m and 1 m the difference is approximately 30 % of that between 1.00 m and 0.01 m.

In summary, the restrictions imposed by MOST and NO<sub>x</sub> measurement uncertainty justify placing inlets at 0.01 and 1.0 m and lead to the removal of 36.1 % (579 values) of all available flux estimates.

The total uncertainty of the 10-min NO<sub>x</sub> flux values due to random error in [ $c(z_2) - c(z_1)$ ] (31 %),  $u_*$  (3 % after Bauguitte et al. (2012)) and measurement height (error in  $\ln z_2/z_1$  of  $\sim 7\%$ ) amounts to 32 %. This reduces to 13 % when considering 1-h flux averages. Note that the uncertainty in  $u_*$  was determined previously at Halley based on the relative difference of 10 min averages of  $u_*$  measured at 4 m over a distance of 100 m (Bauguitte et al., 2012). This might be at the lower end of the true variability in  $u_*$  over 1.2 km distance, however given the very homogeneous and flat snow surface at Dome C it is considered a realistic estimate.

## 2.4 Atmospheric stability

Atmospheric stability is analysed using the Monin-Obukhov length ratio  $z/L$  based on turbulence measurements, with sonic anemometer height  $z$ , and the bulk Richardson number  $Ri_b$  based on temperature and wind profiles and therefore not subject to the assumptions of MOST (Jacobson, 1999):

$$Ri_b = \frac{g[\theta_v(z_2) - \theta_v(z_1)](z_2 - z_1)}{\theta_v(z_1)[u(z_2)^2 + v(z_2)^2]} \quad (8)$$

with gravitational acceleration  $g$ , potential virtual temperature  $\theta_v$ , measurement heights  $z_1$  and  $z_2$ , and horizontal wind speed components  $u$  and  $v$ . Wind speed measurements at 3.3 m were scaled to  $z_2 = 1$  m assuming a logarithmic wind profile and by definition wind speed at  $z_1 = 0$  m is zero.

## 2.5 Modelling nitrate photolysis in snow

Potential  $\text{NO}_2$  production rates from the main  $\text{NO}_3^-$  photolysis channel in snow (Reaction R10) for Dome C conditions are modelled as described in detail in France et al. (2011). Briefly, the radiation transfer model TUV-snow (Lee-Taylor and Madronich, 2002) is used to calculate photolysis rate constants of nitrate in snow  $j_{\text{NO}_3^-}$  as a function of solar zenith angle  $\theta$  and snow depth  $z$ :

$$j_{\text{NO}_3^-} = \int_{\lambda_2}^{\lambda_2} \sigma_a(\lambda, T) \phi(\lambda, T) I(\lambda, \theta, z) d\lambda \quad (9)$$

where  $\sigma_a$  is the absorption cross section of aqueous nitrate after Chu and Anastasio (2003),  $\lambda$  is the wavelength,  $T$  is the temperature,  $\phi$  is the quantum yield for nitrate photolysis on ice after Chu and Anastasio (2003) and  $I$  is the actinic flux.  $I$  was modelled using observed  $\text{O}_3$  columns and assuming a standard atmosphere under clear-sky conditions. Clouds were accounted for by scaling modeled  $I$  to broad band UV measurements. The snow depth dependency of  $I$  was measured at Dome C during this study (France et al., 2011). The depth integrated  $\text{NO}_2$  flux  $F_{\text{NO}_2}$  is computed with

$$F_{\text{NO}_2} = \int_{z=0\text{m}}^{z=1\text{m}} [\text{NO}_3^-] j_{\text{NO}_3^-} d\lambda \quad (10)$$

where  $[\text{NO}_3^-]$  is the amount of nitrate per unit volume of snow. During this study several snow profiles of density and  $\text{NO}_3^-$  concentration were measured within the clean-air sector, with details on snow sample collection and chemical analysis reported in France et al. (2011).

During the 2010–2011 field season surface snow at Dome C was also analysed repeatedly for nitrite ( $\text{NO}_2^-$ ). The effect of chemical loss was minimised by placing the sampled snow into bottles already containing the reagents used for analysis, but concentrations were consistently below the LOD

of 0.5 ppbw. These findings were used to model an upper limit of  $\text{NO}$  production from nitrite ( $\text{NO}_2^-$ ) photolysis (Reaction R12). Photolysis rates  $j_{\text{NO}_2^-}$  were obtained by replacing  $\sigma_a$  and  $\phi$  in Eq. (9) with respective values after Chu and Anastasio (2007) and  $F_{\text{NO}}$  then calculated using  $j_{\text{NO}_2^-}$  and  $[\text{NO}_2^-]$  in Eq. (10) with 0.5 ppbw as an upper limit.

## 3 Results and discussion

This study reports first observations of  $\text{NO}_2$  in the interior of Antarctica and the longest  $\text{NO}_x$  flux measurements above Antarctic snow. Mixing ratios of atmospheric  $\text{NO}$  and  $\text{NO}_2$  were measured at up to three levels above the snow surface from 10 December 2009 to 28 January 2010 (Figs. 3, 4) and show at 1.0 m for the entire season a median of 84 and 71 pptv, respectively (Table 2). The highest mixing ratios are detected in firn interstitial air and systematically decrease with sampling height above the snow surface (Figs. 3, 4). For example, median levels of  $\text{NO}_x$  were 165, 137 and 124 pptv at 0.01, 1.0 and 4.0 m, respectively, whereas the median of available samples in firn air was 386 pptv (Table 2).

Comparison to other sites shows that  $\text{NO}_x$  mixing ratios at Dome C are enhanced. For example, from 10 December 2009 to 28 January 2010 the range of median  $\text{NO}$  mixing ratios between 4.0 and 0.01 m is with 77–90 pptv (Table 2) an order of magnitude higher than at other polar sites (Halley, Neumayer, Alert, Barrow or Summit, as reviewed in Grannas et al., 2007), but similar to those observed on an airborne campaign across East Antarctica and at South Pole during some summer seasons (Table 3). On a seasonal time scale the two-week medians of atmospheric mixing ratios of  $\text{NO}$  at 1 m are with 120 pptv highest before the summer solstice (1–15 December) and decrease in the second half of December and January to lower values ranging between 75 and 81 pptv (Table 3). At South Pole maximum atmospheric mixing ratios of  $\text{NO}$  were also observed before 21 December, except in 1998 (Table 3).

### 3.1 Diurnal variability of $\text{NO}_x$ and boundary layer stability

The major difference to South Pole is the presence of a pronounced diurnal cycle of  $\text{NO}$  and  $\text{NO}_2$  out of phase with solar radiation, with a daily minimum occurring around local noon and a maximum in the evening/night time hours (Figs. 4, 5a–b). Build up and decay of the daily maximum mixing ratios follow on calm days a repeatable pattern, with changes always starting at the lowest intake level followed by those aloft (Fig. 4b–c). On a number of days in December and more frequently in January  $\text{NO}_x$  mixing ratios decreased and the diurnal cycle was suppressed concurrent with wind speeds above  $5 \text{ m s}^{-1}$  (Fig. 3). If the photolytic snow source of  $\text{NO}_x$  was the main driver of atmospheric concentrations one might expect  $\text{NO}_x$  mixing ratios to follow more closely

**Table 3.** Median NO mixing ratios (pptv) on the Antarctic Plateau.

Site	$z$ , m	16–30 Nov	1–15 Dec	16–31 Dec	1–15 Jan	16–31 Jan
Dome C						
NITEDC 2009 <sup>a</sup>	0.01	–	–	123 (3.0)	86 (5.5)	84 (4.1)
	1.0	–	120 (3.8)	81 (8.6)	78 (5.9)	75 (4.9)
	4.0	–	–	100 (2.5)	77 (3.0)	63 (2.2)
South Pole						
ISCAT 1998 <sup>b</sup>	10.0	–	209	237	–	–
ISCAT 2000 <sup>b</sup>	10.0	93	82	88	–	–
ANTCI 2003 <sup>b</sup>		529	164	76	–	–
ANTCI 2005 <sup>c</sup>	0–50	–	95	–	–	–
	51–150	–	90	–	–	–
	151–500	–	30	–	–	–

<sup>a</sup> This study. Values in parenthesis are total sample time in days estimated as the sum of all 1-min intervals;

<sup>b</sup> values from Table 3 in Eisele et al. (2008);

<sup>c</sup> values from Plateau flights of the airborne campaign (Table 3 in Slusher et al., 2010).

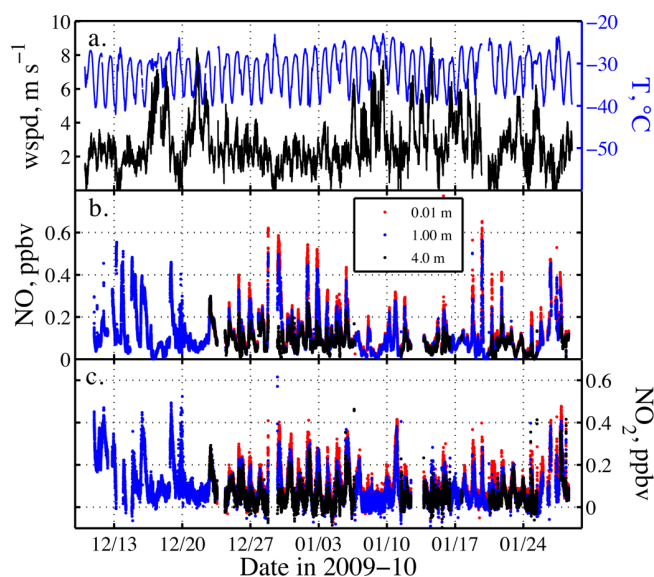


**Fig. 3.** Atmospheric mixing ratios of NO and NO<sub>2</sub> at three heights above the snow and meteorological conditions (wind speed (wspd) at 3.3 m and air temperature  $T$  at 1.6 m) at Dome C in summer 2009–2010.

solar irradiance. However, the peculiar asymmetry of the daily NO<sub>x</sub> maximum with respect to solar noon (Figs. 4b–c, 5a–b) indicates a dominant role of the boundary layer in controlling concentrations of chemical gas phase species emitted from surface snow as suggested previously (King et al., 2006; Anderson and Neff, 2008). Therefore physical boundary layer variables at Dome C are evaluated in more detail.

At Dome C, air temperature and wind speed exhibit a clear diurnal cycle (Figs. 3a, 4a) as reported previously (King et al., 2006). The air temperature shows a daily maximum in the early afternoon, lagging that of solar radiation by about 2 h, and has a diurnal amplitude of  $\sim 12$  K (Fig. 4a).

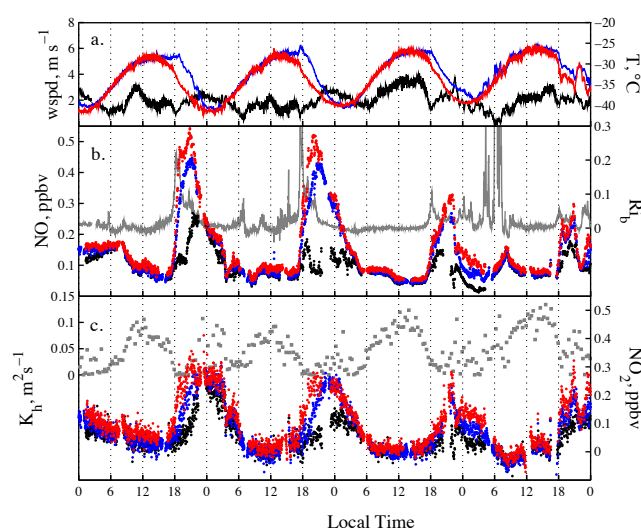


**Fig. 4.** Diurnal variability during 1–4 January 2010: (a) wind speed (wspd) at 3 m (black line), temperatures ( $T$ ) of air at 1 m (blue line) and the snow surface (red line), (b) NO mixing ratios at three heights and bulk Richardson number ( $Ri_b$ ) (grey line) and (c) NO<sub>2</sub> mixing ratios at three heights and turbulent diffusion coefficient of heat ( $K_h$ ) at 1 m (grey symbols). Mixing ratios at 0.01, 1.0 and 4.0 m are shown as red, blue and black symbols, respectively.

The wind speed peaks around noon, decreases sharply in the early evening ( $\sim 18:00$  LT), but picks up again during night time (18:00–06:00 LT), with a rather small diurnal amplitude of  $\sim 1.5$  m s<sup>-1</sup> (Fig. 4a). Diurnal variations of both variables are typical for locations where a convective boundary layer develops as a response to daytime heating (King et al., 2006). Wind direction also shows a small but significant diurnal cycle (data not shown). Winds were from 190–200° during 10:00–14:00 LT and then shift to  $\sim 220^\circ$  during 18:00–24:00 LT. Both increase in wind speed and change of wind direction later in the evening suggest development of an Ekman

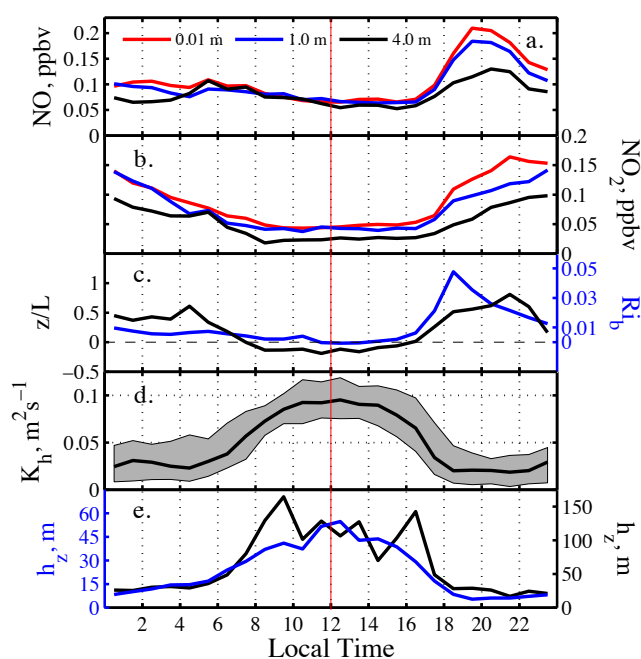


**Fig. 5.** The asymmetry in diurnal cycles of mixing ratios and physical boundary layer variables with respect to local noon (vertical red line): (a) NO mixing ratios, (b) NO<sub>2</sub> mixing ratios, (c) atmospheric stability as expressed by the Monin-Obukhov length ratio  $z/L$ , with sonic anemometer height  $z$ , and bulk Richardson number  $Ri_b$ , (d) turbulent diffusion coefficient of heat  $K_h$  at 1 m and (e) boundary layer height  $h_z$  estimated after Pollard et al. (1973) (blue line) and Zilitinkevitch et al. (2002) (black line); note different y-axis scales. Lines represent median values and shaded areas the range between the 0.25 and 0.75 percentiles of 1-hourly bins during 22 December 2009–28 January 2010.

spiral similar to previous observations on the East Antarctic Ice sheet (Kuhn et al., 1977). Gradients of temperature and wind speed show an asymmetric diurnal cycle similar to that of NO<sub>x</sub> mixing ratios (Fig. 4). For example, during the relatively calm period 1–4 January 2010 near-surface gradients of temperature, i.e. between 1 m and the snow surface, are consistently larger in the evening than in the morning with warming and cooling of air always initiating at the surface (Fig. 4a). Similarly, the wind speed increase in the morning is more gradual than its drop in the early evening (Fig. 4a).

Parameters of atmospheric stability, the Monin-Obukhov length ratio  $z/L$  and the bulk Richardson number  $Ri_b$ , were derived to investigate this further.  $L$  is a height proportional to the height above the surface at which buoyancy first dominates wind shear, whereas  $Ri_b$  describes the ratio of turbulence due to buoyancy (free convection) relative to that due to shear (forced convection) (Eq. 8). The median diurnal cycle of  $z/L$  during the study period suggests that between 07:00 and 16:00 LT the boundary layer becomes unstable and convective ( $z/L < 0$ ), whereas during the rest of the day stable stratification prevails ( $z/L > 0$ ) (Fig. 5c), consis-

tent with previous micrometeorological measurements (Argentini et al., 2005; King et al., 2006).  $Ri_b$  values are positive throughout most of the day, indicating stable conditions (Figs. 4b, 5c). Small and negative  $Ri_b$  values around solar noon indicate that the atmosphere has become unstable with most turbulence from wind shear, but some contributions also from buoyancy (Figs. 4b, 5c). On the one hand,  $Ri_b$  values significantly underestimate the daily duration of convective behaviour when compared to  $z/L$  or existing observations (Argentini et al., 2005). This can be attributed to systematic errors in the calculation of  $Ri_b$  due to uncertainty in the temperature gradients. This is the case during near neutral and unstable conditions when gradients are small compared to the temperature measurement error of  $\sim 0.1^\circ\text{C}$ . During stable conditions this should be less important. On the other hand,  $Ri_b$  tracks NO<sub>x</sub> mixing ratios very well: in the early evening  $Ri_b$  rises sharply to a maximum around 18:30 LT, coinciding with a drastic increase in NO<sub>x</sub> mixing ratios (Figs. 4b–c, 5a–c). The increase illustrates the drop in wind shear concurrent with a strong temperature inversion at the surface. Turbulent flow is very reduced, possibly even to laminar flow. Later,  $Ri_b$  decreases again as wind shear grows, leading to upward mixing of NO<sub>x</sub> accumulated near the ground. NO mixing ratios decrease sooner and at a quicker rate than mixing ratios of NO<sub>2</sub> (Figs. 4, 5) leading to maximum NO<sub>2</sub> : NO ratios during night time. The difference in dynamics between the two chemical species likely reflects that NO<sub>2</sub> : NO ratios shift to a new equilibrium during night time, i.e. NO<sub>2</sub> dilution from mixing is in part offset by a reduction in its photolytic sink (Reaction R1), whereas NO dilution is further enhanced by a reduction in its photolytic source (Reaction R1).

For air chemistry modelling the most significant physical variables of the boundary layer are the diffusivity  $K$  and height  $h_z$  (Anderson and Neff, 2008). The turbulent diffusion coefficient for heat  $K_h$  (Eq. 4) was calculated at 1 m (Figs. 4c, 5d). Its noon maximum suggests that mixing is strongest around solar noon and has contributions from turbulence due to buoyancy (free convection) since  $z/L < 0$ , whereas during late afternoon to morning (16:00–07:00 LT) the atmosphere is stably stratified ( $z/L > 0$ ) and any turbulence present is due to wind shear (forced convection) as the sole driver of mixing (Fig. 5c, d). Calculated estimates of  $h_z$  also show significant diurnal variability and daily ranges of median  $h_z$  were 5–55 m after Pollard et al. (1973), and 17–165 m after Zilitinkevitch et al. (2002) (Fig. 5e). No direct observations of  $h_z$  are available to validate the estimates. However, sodar records from summer 1999 showed that starting from a shallow nocturnal boundary layer of  $< 50$  m at 07:00 LT a capping inversion reached heights of 200–300 m at 13:00–14:00 LT in late December to early January and disappeared by 18:00 LT leaving behind the nocturnal boundary layer (Argentini et al., 2005; King et al., 2006). The predicted  $h_z$  values appear biased low during daytime, but suggest during the night the existence of a very shallow nocturnal boundary layer with  $h_z < 20$  m (Fig. 5c). This is consistent with visual

observations of a defined layer of haze forming at the ground at Dome C, which indicate that the atmospheric boundary layer does not exceed building height of 20 m during night time.

A previous analysis of the surface energy budget at Dome C in summer provides further detail on the daytime convection. The diurnal sensible heat flux was found to be in upward direction during 06:00–17:00 LT resulting in vigorous convection (King et al., 2006). At its origin is greater partitioning of available energy into the sensible heat flux rather than latent heat because air temperatures and therefore water vapour pressures are low at this location (King et al., 2006). The sensible heat flux is responsible for the large day-night temperature amplitude and drives the development of a convective boundary layer throughout the day, giving rise to efficient vertical mixing (King et al., 2006). The dominant role of mixing for  $\text{NO}_x$  mixing ratios is illustrated by the inverse relationship with  $K_h$  ( $R^2 = 0.54$  for binned data) (Fig. 6a). A similar relationship has been observed previously at South Pole between NO and friction velocity  $u_*$  (Neff et al., 2008). Conversely,  $\text{NO}_x$  mixing ratios are enhanced when the boundary layer is shallow (Fig. 6b), as seen also at South Pole (Neff et al., 2008). It should be noted that  $h_z$  and  $K_h$  are not independent since turbulent diffusivity of the atmosphere controls, with contributions from sensible heat flux, the magnitude of  $h_z$ .

The diurnal cycles of all physical atmospheric variables discussed above ( $z/L$ ,  $Ri_b$ ,  $K_h$ ,  $h_z$ ) are asymmetrical with respect to local noon (Fig. 5). They increase gradually in the morning, whereas they decrease more quickly in the early evening, reflecting the development and collapse of the convective boundary layer. This pattern is similar to the asymmetry in the diurnal  $\text{NO}_x$  cycle, which shows large increases in the evening but lacks a discernible peak in the morning (Fig. 5a, b) and can be explained as follows: since the diurnal cycle of sensible heat flux was observed to be fairly symmetrical around noon (Fig. 10a in King et al., 2006), the asymmetry in the temperature gradients (Fig. 4a) must be then due to differences in diffusivity of heat  $K_h$  between the morning and evening. Small temperature gradients in the morning are consistent with larger  $K_h$  values when compared to the same hour of day in the evening (Figs. 4a, 5d) and illustrate that convection is a very efficient process for the upward mixing of heat. In the evening the downward heat flux is smaller due to comparatively lower diffusivities indicating that heat is more effectively moved away from the snow surface than towards it. At Dome C this is confirmed by the asymmetry in the average diurnal cycle of snowpack heat flux, i.e. the energy flux across the air-snow boundary, which shows a minimum of  $-30 \text{ W m}^{-2}$  at 08:00 LT (outgoing flux) compared to a maximum of  $20 \text{ W m}^{-2}$  at 18:00–23:00 LT (incoming) (Fig. 9 in King et al., 2006). By assuming similarity between  $K_h$  and  $K_c$  the arguments for heat transport apply also to the vertical mixing of  $\text{NO}_x$  emitted at the surface.

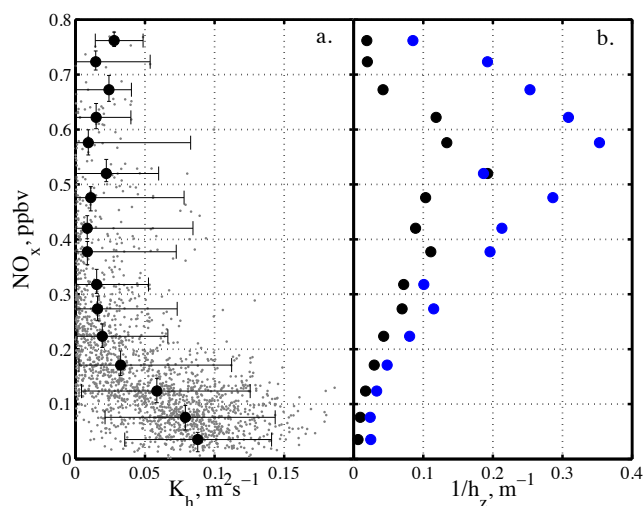


**Fig. 6.** (a) Atmospheric mixing ratios of  $\text{NO}_x$  as a function of the turbulent diffusion coefficient of heat  $K_h$  (both at 1 m). Plotted are 10-min means (grey symbols) and data binned into 50 pptv intervals (median values as black symbols and error bars indicating the 5–95 percentile range). (b) Binned  $\text{NO}_x$  mixing ratios as a function of boundary layer height  $h_z$  estimated after Pollard et al. (1973) (blue symbols) and Zilitinkevitch et al. (2002) (black symbols).

Comparison of diurnal cycles of  $\text{NO}_x$  mixing ratios with Summit, Greenland, and Halley in coastal Antarctica is informative as both sites are located at similar latitudes to Dome C and therefore subject to the same diurnal radiative forcing at the top of the atmosphere. However, at Summit,  $\text{NO}_x$  mixing ratios are not only lower, but show two daily maxima, morning and evening, about equal in size (Thomas et al., 2011), consistent with a diurnal cycle of  $Ri_b$  symmetric with respect to solar noon (Helmig et al., 2002). At Halley, the diurnal cycle of  $\text{NO}_x$  mixing ratios follows with some delay solar irradiance. In contrast to Dome C, no convection occurs and during calm periods the boundary layer height remains almost constant throughout the day (King et al., 2006). Mixing in the boundary layer is exclusively driven by wind shear and depends therefore more on synoptic events (King et al., 2006). The diurnal cycle of  $\text{NO}_x$  mixing ratios is controlled by the snow source and atmospheric halogen mediated chemistry, i.e. formation and uptake of  $\text{BrNO}_3$  and  $\text{INO}_3$ , which prevents build up of  $\text{NO}_x$  (Bauguitte et al., 2012). Atmospheric halogens in coastal Antarctica are thought to originate from the sea ice zone and are therefore expected to play a much less important role further inland.

### 3.2 The $\text{NO}_x$ snow source

The average of all available mixing ratio differences  $\Delta[\text{NO}_x]$  between 1 and 0.01 m was  $-43$  pptv with an average standard error of 9 pptv (Fig. 7a).  $\Delta[\text{NO}_x]$  not significantly different from zero and excluded from the flux estimate were observed typically around local noon, a time of strong atmospheric

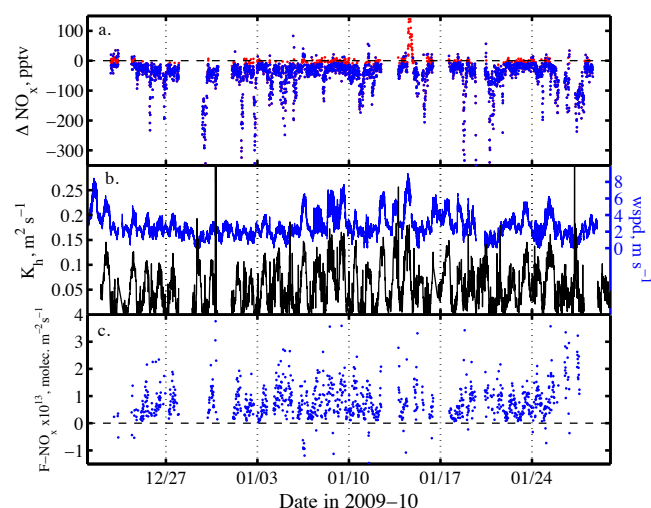


**Fig. 7.** 10-min averages of  $\text{NO}_x$  flux at Dome C in summer 2009–2010 between 1.0 and 0.01 m: (a) difference in  $\text{NO}_x$  mixing ratios ( $\Delta\text{NO}_x$ ) between 1.0 and 0.01 m (blue symbols); values within  $\pm 1\sigma$  standard error were excluded from the flux calculation (red symbols), (b) turbulent diffusion coefficient of heat ( $K_h$ ) at 1 m and wind speed (wspd) at 3 m, and (c)  $\text{NO}_x$  flux ( $F\text{-NO}_x$ ).

mixing (Fig. 7a). From a total of 1023 10-min average flux values ( $\sim 7$  days), 52 % were during stable and the remainder during unstable conditions. Corrections from  $\Phi_h$  (Eq. 5) were  $< 10\%$  when compared to the case of a neutral boundary layer decreasing flux during stable conditions and increasing flux during unstable conditions.  $K_h$  values were on average ( $\pm 1\sigma$ )  $0.054 (\pm 0.043) \text{ m s}^{-1}$  and correlate with horizontal wind speed ( $R = 0.56$ ,  $p < 0.001$ ) (Figs. 4, 7b). The  $\text{NO}_x$  fluxes between 0.01 and 1.0 m were almost exclusively emissions from the snow surface with an average ( $\pm 1\sigma$ ) of  $8.2 (\pm 7.4) \times 10^{12} \text{ molecule m}^{-2} \text{ s}^{-1}$  (Table 2, Fig. 7c).

The 10 min averages of observed  $\text{NO}_x$  flux show some scatter due to noise in  $\Delta[\text{NO}_x]$  and  $K_h$  values, but exhibit a close relationship with UV-A irradiance (Fig. 8), as also seen in the median diurnal cycle for the entire period (Fig. 9b–c). Mixing ratios of  $\text{NO}_x$  in firn air also correlate with surface UV-A irradiance, albeit on some days with a time lag of a few hours (Figs. 8a, 9c). This confirms the existence of a photolytic source of  $\text{NO}_x$  in the upper snowpack, i.e. photolysis of  $\text{NO}_3^-$  in snow. However, the fate of  $\text{NO}_x$  from nitrate photolysis in snow is strongly controlled by boundary layer diffusivity once released from the snowpack. The median  $\text{NO}_x$  flux at noon is  $\sim 2\text{--}3$  times larger than that during night time (Fig. 9b, Table 2), a diurnal pattern that is disrupted by occasional increases in  $K_h$  leading to larger  $\text{NO}_x$  fluxes (Fig. 8). Generally, maximum  $\text{NO}_x$  flux coincides with minimum atmospheric mixing ratios, consistent with the notion that as the boundary layer develops emissions are mixed by turbulence into an increasingly larger volume (Fig. 9). Interestingly, the median diurnal cycle of  $\text{NO}_x$  flux reveals

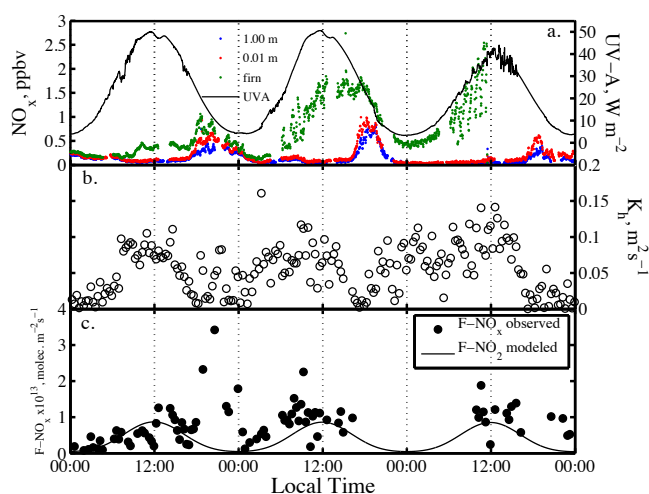


**Fig. 8.** Atmospheric mixing ratios of  $\text{NO}_x$  and snow emissions during 18–21 January 2010. Shown are (a) mixing ratios above the snow and in firn air along with UV-A irradiance, (b) the turbulent diffusion coefficient of heat  $K_h$  at 1 m and (c) observed  $\text{NO}_x$  flux compared to modelled potential  $\text{NO}_2$  flux from nitrate photolysis (Reaction R10).

a small secondary maximum during the night (23:00–03:00 LT) (Fig. 9b). A likely mechanism is that wind shear generated turbulence during night time drives snow pack ventilation of  $\text{NO}_x$  which had accumulated beforehand when the boundary layer was very stable.

Assuming that  $\text{NO}_x$  snow emissions are uniformly mixed throughout the boundary layer and that in continental Antarctica, away from potential halogen sources the main  $\text{NO}_x$  sink is the reaction with hydroxyl radicals (Reaction R8), one can calculate  $\text{NO}_x$  production rates based on the estimated surface flux  $F_{\text{NO}_x}$  with

$$\frac{d[\text{NO}_x]}{dt} \sim \frac{F_{\text{NO}_x}}{h_z} - k_{\text{R8}}[\text{NO}_2][\text{OH}] \quad (11)$$

We assume boundary layer heights  $h_z$  of 250 m during the day based on previous sodar records (Argentini et al., 2005) and 10 m during night time following the estimate after Pollard et al. (1973). The reaction rate constant  $k_{\text{R8}}$  is calculated for Dome C conditions according to recommendations listed in Sander et al. (2006). Measured  $\text{NO}_2$  is used, whereas OH is set to a constant value of  $2.0 \times 10^6 \text{ molecule cm}^{-3}$ , which equals the 16–31 December mean at South Pole in 1998 and 2000 (Eisele et al., 2008). With Eq. (11) average  $\text{NO}_x$  production rates of 4 and 98  $\text{pptv h}^{-1}$  are obtained at local noon (11:30–12:30 LT) and midnight (23:30–00:30 LT), respectively. Lower  $\text{NO}_x$  production at noon than midnight indicates that the increase in boundary layer depth during the day offsets by far the concurrent increase in emission. Night time  $\text{NO}_x$  production is of the order of magnitude needed to explain the steep evening rise of  $\text{NO}_x$  concentrations from 110 to 300 pptv in about 2 h (Fig. 9a). These results are

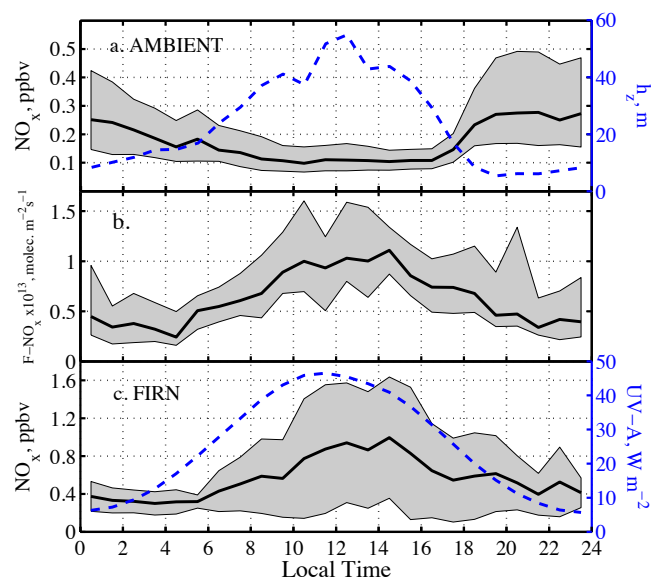


**Fig. 9.** The diurnal cycle of  $\text{NO}_x$  atmospheric mixing ratios and flux during 22 December 2009–28 January 2010: (a)  $\text{NO}_x$  mixing ratios at 1 m with boundary layer height  $h_z$  estimated after Pollard et al. (1973), (b) observed  $\text{NO}_x$  flux ( $F\text{-NO}_x$ ) between 0.01 and 1 m and (c)  $\text{NO}_x$  mixing ratios in firn air from occasional sampling (Table 2) and UV-A irradiance at 1 m. Lines are median values and shaded areas the 25–75 percentile range of 1-hourly bins; except  $\text{NO}_x$  in firn air is average  $\pm 1\sigma$ .

sensitive to the assumed values of  $h_z$  and OH mixing ratios. For example, chemical loss rates from the right hand term in Eq. (11) were  $3 \text{ pptv h}^{-1}$  at noon and  $13 \text{ pptv h}^{-1}$  at midnight. These change to  $5 \text{ pptv h}^{-1}$  at noon and  $6 \text{ pptv h}^{-1}$  at midnight, if one assumes the same daily average OH, but the presence of a diurnal cycle with a noontime maximum of  $3.0 \times 10^6 \text{ molecule cm}^{-3}$  and a midnight minimum of  $1.0 \times 10^6 \text{ molecule cm}^{-3}$ . Concurrent measurements of  $\text{HO}_x$  radicals are needed to further evaluate the  $\text{NO}_x$  sink including reaction with peroxy radicals  $\text{NO}_2 + \text{HO}_2$  ( $\text{RO}_2$ ). Nevertheless, the above suggests that the photolytic snow source has a significant impact on atmospheric  $\text{NO}_x$  concentrations, especially during times of the day when the boundary layer becomes very shallow (Fig. 9). This is also consistent with independent measurements of the stable isotopic composition of atmospheric particulate nitrate at Dome C, which show on a seasonal time scale a clear signature of snow emissions from nitrate photolysis (Frey et al., 2009b).

Instrumentation and methods to estimate flux vary considerably between sites (e.g. Bauguitte et al., 2012) and therefore the use of inter-site comparisons to test the current model of the  $\text{NO}_x$  snow source remains difficult. For example, average and noon  $\text{NO}_x$  flux estimated at Halley on 2 February 2005 were  $7.3 \times 10^{12}$  and  $12.6 \times 10^{12} \text{ molecule m}^{-2} \text{ s}^{-1}$ , respectively (Bauguutte et al., 2012). However, the latter study simplified flux estimates by lin-

earizing the logarithmic concentration profile, which can induce significant error depending on the inlet heights. Recalculation of the Halley data with Eq. (5) for neutral conditions yields  $\sim 20\%$  smaller values, i.e.  $5.9 \times 10^{12}$  and  $10.2 \times 10^{12} \text{ molecule m}^{-2} \text{ s}^{-1}$ , respectively. At South Pole (2835 m) average  $\text{NO}_x$  flux during 26–30 November 2000 was  $3.9 \times 10^{12} \text{ molecule m}^{-2} \text{ s}^{-1}$  (Oncley et al., 2004). It should be borne in mind that this study measured only NO gradients and inferred  $\text{NO}_x$  flux based on atmospheric photochemical considerations (Oncley et al., 2004). Thus, it appears that the seasonal and noon average  $\text{NO}_x$  flux at Dome C of  $8.2 \times 10^{12}$  and  $9.4 \times 10^{12} \text{ molecule m}^{-2} \text{ s}^{-1}$  (Table 2) belong to the largest values reported so far from Antarctica and even the Arctic (see overview in Bauguutte et al., 2012).

Observed  $\text{NO}_x$  flux was compared with model calculations of potential  $\text{NO}_x$  production from nitrate photolysis in snow. Using only the main  $\text{NO}_3^-$  photolysis channel (Reaction R10) yielded a median model:observation ratio of 0.66. When NO production from  $\text{NO}_2^-$  photolysis (Reaction R12) was included, assuming a maximum  $\text{NO}_2^-$  concentration in snow of 0.5 ppbw, the median model:observation ratio increased to 0.91. Comparison of the median diurnal cycles of modeled and observed  $F_{\text{NO}_x}$  including respective uncertainties reveals that the model underpredicts observations significantly from early evening to morning (18:00–03:00 LT) (Fig. 10). This holds also true when model uncertainties due to the spatial variability in  $\text{NO}_3^-$  snow profiles of  $\pm 24\%$  are taken into account (Fig. 10). However, during the remainder of the day the model matches observations within the rather large uncertainties (Fig. 10).

The night time discrepancy between model and observations highlights uncertainties and processes neglected in this simple parameterisation of the  $\text{NO}_x$  snow source. First, including chemical sink reactions of  $\text{NO}_x$  (e.g. Reactions R8–R9) and deposition within the snowpack will further decrease modeled  $F_{\text{NO}_x}$ , but requires observational constraints on peroxy and halogen radical levels in firn air. Second, adding vertical transport of photolysis products within and above the snow pack in the absence of secondary chemical reactions will change the shape of the median diurnal cycle of  $F_{\text{NO}_x}$  but not its daily mean value. Observations discussed above underline the importance of this process as the night time increase in wind shear likely causes enhanced upward ventilation of  $\text{NO}_x$  which had been temporarily accumulated in the upper snow pack during very stable conditions. And third, the quantum yield of  $\text{NO}_3^-$  photolysis in natural snow still presents a major uncertainty. It characterises the so-called cage effect, i.e. the tendency of the ice matrix to trap reaction products. A recent lab study found that the quantum yield for photolysis of  $\text{HNO}_3$  adsorbed to the surface of ice films is close to unity (Zhu et al., 2010), whereas that of  $\text{NO}_3^-$  measured by Chu and Anastasio (2003) on artificial ice pellets and used in the model calculation is three orders of magnitude smaller. Thus, the efficiency of nitrate photolysis and

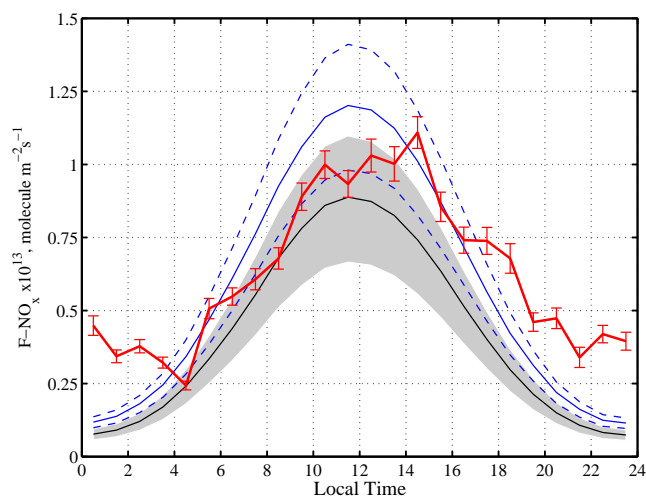


**Fig. 10.** The median diurnal variation of  $\text{NO}_x$  flux ( $F\text{-NO}_x$ ) at Dome C compared to model calculations:  $F\text{-NO}_x$  during 22 December 2009–28 January 2010 observed between 0.01 and 1 m (red line) and its uncertainty (error bars indicating the  $1\text{-}\sigma$  standard error of the median calculated as  $1.253 \sigma/\sqrt{N}$ , where  $\sigma$  is the random error of 10-min flux values and  $N$  is the number of samples per 1-h bin, e.g. Maindonald and Braun, 2003). Modeled  $F\text{-NO}_x$  during 22 December 2009–21 January 2010 from  $\text{NO}_3^-$  photolysis only (Reaction R10, black line) and including also contributions from  $\text{NO}_2^-$  photolysis (Reaction R12) assuming a maximum  $\text{NO}_2^-$  concentration in snow of 0.5 ppbw (blue line). The shaded area and dashed lines show the range of  $F\text{-NO}_x$  due to the spatial variability in  $\text{NO}_3^-$  snow profiles at Dome C reported in France et al. (2011).

therefore modelled  $\text{NO}_x$  flux are highly sensitive to the location of nitrate in the snow grain and experimental constraints are crucial to model improvement.

### 3.3 The $\text{NO}_2 : \text{NO}$ ratio and potential radical concentrations

Atmospheric  $\text{NO}_2 : \text{NO}$  ratios observed at Dome C are  $< 1$  during daytime and  $> 1$  during nighttime, similar to observations at Halley (Fig. 11). Interestingly,  $\text{NO}_2 : \text{NO}$  ratios show a strong height dependency (Fig. 11), i.e. their median values decrease from 1.5 in firm air to 0.6–0.8 in air above the snow surface (Table 2). A comparison to predicted steady-state ratios can provide an estimate of concentrations for oxidants other than  $\text{O}_3$  such as peroxy and halogen radicals. The steady-state assumption might not apply since significant snow emissions predominantly in the form of  $\text{NO}_2$  can shift the  $\text{NO}_2 : \text{NO}$  ratio, i.e. converting the average observed  $\text{NO}_x$  flux to a volumetric production rate yields values of the same order of magnitude as  $\text{NO}_2$  formation via Reaction (R3), especially when the air is stably stratified. However, a closer examination of the median  $\text{NO}_2 : \text{NO}$  ratios reveals that they are very similar at the 1.0 m and 4.0 m level throughout the day, whereas at 0.01 m and in firm air they

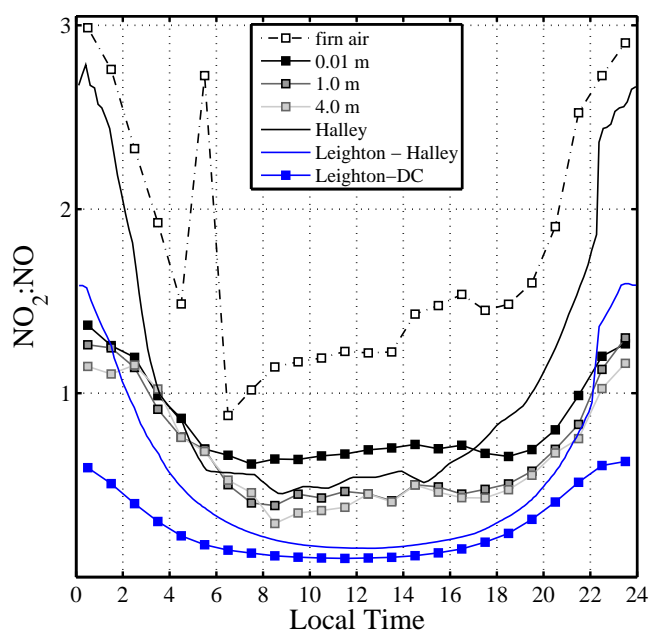


**Fig. 11.** The median diurnal cycle of the  $\text{NO}_2 : \text{NO}$  ratio during 22 December 2009 to 28 January 2010 shows significant deviations from Leighton steady-state at Dome C. Halley observations (black line) are shown for comparison (Bauguitte et al., 2012).

differ, especially during daytime when the  $\text{NO}_x$  flux reaches its maximum (Fig. 11). The ratios are therefore suggested to be perturbed by photolytic  $\text{NO}_2$  release in firm air and at the snow surface, but likely reach a pseudo steady-state after transport of some distance away from the snow source, i.e. here to the 1.0 m level.

Atmospheric  $\text{NO}_2 : \text{NO}$  ratios can be calculated using an extended Leighton mechanism as derived in Ridley et al. (2000). For small carbon number peroxy radicals ( $\text{RO}_2$ )  $k_{\text{R}4} \sim k_{\text{R}6}$  and for  $\text{XO}=\text{BrO}$ ,  $\text{ClO}$   $k_{\text{R}4} \sim 0.5k_{\text{R}7}$ . The ratios can then be written as:

$$\frac{[\text{NO}_2]}{[\text{NO}]} = \frac{k_{\text{R}3}[\text{O}_3] + k_{\text{R}4}[\text{OX}]}{j_{\text{NO}_2}} \quad (12)$$

where the total radical concentration  $[\text{OX}] = [\text{HO}_2] + [\text{RO}_2] + 2[\text{XO}]$ .  $\text{NO}_2$  photolysis rate constants  $j_{\text{NO}_2}$  were calculated with TUV-snow (Lee-Taylor and Madronich, 2002). Simple Leighton steady-state ratios ( $[\text{OX}] = 0$ ) deviate significantly from observations, and they do so more strongly than at Halley (Fig. 11). Inserting the observed average  $\text{NO}_2 : \text{NO}$  ratio into Eq. (12) yields a season mean for  $[\text{OX}]$  at 1 m of  $6.3 \times 10^8 \text{ molecule m}^{-3}$  (33 pptv), a value about 9 times the  $[\text{HO}_2] + [\text{RO}_2]$  observed at South Pole (Eisele et al., 2008) and 3 times of  $[\text{HO}_2] + [\text{RO}_2]$  seen at Summit (Sjostedt et al., 2007). Including observed levels of halogen radicals  $\text{BrO}$  and  $\text{IO}$  into Eq. (12) explained the shift in  $\text{NO}-\text{NO}_2$  partitioning in coastal Antarctica (Bauguitte et al., 2012). However, even if  $\text{BrO}$  and  $\text{IO}$  were occasionally present at Dome C, coastal levels of  $\sim 5$  pptv would be too low to explain a significant

part of the inferred total radical concentration [OX]. Thus, the  $\text{NO}_2 : \text{NO}$  ratios suggest that peroxy and other radical levels in the boundary layer of Dome C are either significantly higher than measured elsewhere in the polar regions or other processes leading to enhanced  $\text{NO}_2$  have to be invoked.

#### 4 Conclusions

$\text{NO}_x$  measurements at Dome C, including first observations of  $\text{NO}_2$  on the Antarctic Plateau, confirm previous findings from South Pole that in summer  $\text{NO}_x$  mixing ratios in the regional lower troposphere are enhanced compared to coastal Antarctica, and therefore are very likely typical for the larger East Antarctic Ice Sheet (Table 3). Meaningful site inter-comparisons of atmospheric  $\text{NO}_x$  and other chemical species with a snow source need to take into account not only season or latitude but also measurement height, since vertical gradients of mixing ratios can be significant, especially during times when the air is stably stratified. A steady-state analysis of  $\text{NO}_2 : \text{NO}$  ratios suggests that mixing ratios of peroxy radicals are possibly higher than any previous observations in air above polar snow and is consistent with the notion of a highly oxidising canopy enshrouding the East Antarctic Plateau in summer.

The characteristic diurnal cycle of  $\text{NO}_x$  mixing ratios at Dome C is strongly asymmetric with respect to solar noon, i.e. a maximum in the early evening but lack thereof in the morning. This can be explained by the daily development of a convective boundary layer starting in the early morning hours and reaching maximum heights in the early afternoon. Efficient convective upward mixing of  $\text{NO}_x$  emitted by the surface snow and the concurrent increase in boundary layer height cause dilution of atmospheric concentrations, which by far exceeds the daytime increase in  $\text{NO}_x$  production from nitrate photolysis in snow. Therefore  $\text{NO}_x$  mixing ratios show a minimum around solar noon and no morning peak. In the early evening strong radiative cooling and a temporary decrease in wind shear during the decay of the convective boundary layer lead to accumulation of  $\text{NO}_x$  emitted by the snow pack near the surface and formation of the daily  $\text{NO}_x$  maximum. Atmospheric mixing ratios decrease later in the evening, when wind shear and therefore atmospheric diffusivity increase slightly resulting in upward venting of  $\text{NO}_x$ . In summary, at Dome C diffusivity and height of the boundary layer have a strong control on the diurnal cycle of  $\text{NO}_x$  mixing ratios and likely any other chemical tracer with a surface source.

The questions arises how representative the diurnal  $\text{NO}_x$  cycle is for the East Antarctic Plateau region. The magnitude of the diurnal variation in radiative forcing at Dome C is at the upper end of the range possible in East Antarctica, while South Pole is a geographical singularity with no diurnal variability at all. It has been argued previously that the

convective boundary layer observed at Dome C is not typical for East Antarctica, as daytime convection will always grow weaker both North and South of  $75^\circ \text{S}$  (King et al., 2006). This implies that the diurnal cycle in boundary layer height is dampened leading to a less extreme diurnal amplitude in  $\text{NO}_x$  mixing ratios when moving away from Dome C. While Dome C might be an extreme case, this work confirms that air chemistry modelling of chemical species with a photochemical or physical surface source requires an accurate description of atmospheric boundary layer dynamics. Accurate modelling of the boundary layer above the polar ice sheets will not only benefit 1-D atmosphere–snow models to match boundary layer structure, chemical composition and flux above snow (e.g. Thomas et al., 2011; Brun et al., 2011), but also global climate models (e.g. Genthon et al., 2010).

Currently known factors leading to enhanced  $\text{NO}_x$  concentrations above the East Antarctic Plateau region in summer are 24 h of continuous sunlight, a shallow boundary layer, location at the bottom of a large air drainage basin and low temperatures reducing primary production rates of  $\text{HO}_x$  radicals (Davis et al., 2008). In addition,  $\text{NO}_x$  emissions from snow at Dome C were found to be among the highest observed in Antarctica and the Arctic, and thus contribute to high  $\text{NO}_x$  mixing ratios in the boundary layer above the East Antarctic Plateau.

A simple nitrate photolysis model matches the observed median diurnal  $\text{NO}_x$  flux during the day but has significant low bias during the night. The difference is significant taking into account the total random error in flux observations and model uncertainties due to the variability of  $\text{NO}_3^-$  concentrations in snow and potential contributions from  $\text{NO}_2^-$  photolysis. The quantum yield of nitrate photolysis in natural snow, which reflects the location of the nitrate ion in snow grains, remains a large model uncertainty and needs to be better constrained by observations. This will benefit model parameterisations of the  $\text{NO}_x$  snow source above Antarctica and other snow covered areas.

*Acknowledgements.* This work has been made possible thanks to partial support by Institut Paul Émile Victor (IPEV – Programme 1011 NITEDC). MMF is funded by the Natural Environment Research Council through the British Antarctic Survey Polar Science for Planet Earth Programme. We acknowledge also support by the French national atmospheric program LEFE-CHAT managed by INSU/CNRS. Sonic data were provided by C. Genthon, LGGE (IPEV – Programme 1013 and OSUG CENACLAM observatory) and Eric Fossat, OCA. We thank B. Jourdain and the IPEV – Programme CESOA for providing ozone data, PNRA for meteorological data and IPEV for logistic support. JLF and MDK wish to thank NERC for support under grants NE/F0004796/1 and NE/F010788 and NERC FSF through grants S55.0608 and S84.0609 and RHUL research strategy fund awards.

Edited by: I. Trebs

## References

- Anderson, P. S. and Neff, W. D.: Boundary layer physics over snow and ice, *Atmos. Chem. Phys.*, 8, 3563–3582, doi:10.5194/acp-8-3563-2008, 2008.
- Argentini, S., Viola, A., Sempreviva, A. M., and Petenko, I.: Summer boundary-layer height at the plateau site of Dome C, Antarctica, *Bound.-Lay. Meteorol.*, 115, 409–422, doi:10.1007/s10546-004-5643-6, 2005.
- Bartels-Rausch, T., Jacobi, H.-W., Kahan, T. F., Thomas, J. L., Thomson, E. S., Abbatt, J. P. D., Ammann, M., Blackford, J. R., Bluhm, H., Boxe, C., Domine, F., Frey, M. M., Gladich, I., Guzmán, M. I., Heger, D., Huthwelker, Th., Klán, P., Kuhs, W. F., Kuo, M. H., Maus, S., Moussa, S. G., McNeill, V. F., Newberg, J. T., Pettersson, J. B. C., Roeselová, M., and Sodeau, J. R.: Relationship between snow microstructure and physical and chemical processes, *Atmos. Chem. Phys. Discuss.*, 12, 30409–30541, doi:10.5194/acpd-12-30409-2012, 2012.
- Bauguitte, S. J.-B., Bloss, W. J., Evans, M. J., Salmon, R. A., Anderson, P. S., Jones, A. E., Lee, J. D., Saiz-Lopez, A., Roscoe, H. K., Wolff, E. W., and Plane, J. M. C.: Summertime NO<sub>x</sub> measurements during the CHABLIS campaign: can source and sink estimates unravel observed diurnal cycles?, *Atmos. Chem. Phys.*, 12, 989–1002, doi:10.5194/acp-12-989-2012, 2012.
- Brun, E., Six, D., Picard, G., Vionnet, V., Arnaud, L., Bazile, E., Boone, A., Bouchard, A., Genthon, C., Guidard, V., Le Moigne, P., Rabier, F., and Seity, Y.: Snow/atmosphere coupled simulation at Dome C, Antarctica, *J. Glaciol.*, 57, 721–736, doi:10.3189/002214311797409794, 2011.
- Chu, L. and Anastasio, C.: Quantum yields of hydroxyl radical and nitrogen dioxide from the photolysis of nitrate on ice, *J. Phys. Chem. A*, 107, 9594–9602, 2003.
- Chu, L. and Anastasio, C.: Temperature and wavelength dependence of nitrite photolysis in frozen and aqueous solutions, *Environ. Sci. Technol.*, 41, 3626–3632, doi:10.1021/es062731q, 2007.
- Cohen, L., Helmig, D., Neff, W. D., Grachev, A. A., and Fairall, C. W.: Boundary-layer dynamics and its influence on atmospheric chemistry at Summit, Greenland, *Atmos. Environ.*, 41, 5044–5060, doi:10.1016/j.atmosenv.2006.06.068, 2007.
- Crawford, J. H., Davis, D. D., Chen, G., Buhr, M., Oltmans, S., Weller, R., Mauldin, L., Eisele, F., Shetter, R., Lefer, B., Arimoto, R., and Hogan, A.: Evidence for photochemical production of ozone at the South Pole surface, *Geophys. Res. Lett.*, 28, 3641–3644, 2001.
- Davis, D. D., Chen, G., Buhr, M., Crawford, J., Lenschow, D., Lefer, B., Shetter, R., Eisele, F., Mauldin, L., and Hogan, A.: South Pole NO<sub>x</sub> chemistry: an assessment of factors controlling variability and absolute levels, *Atmos. Environ.*, 38, 5275–5388, doi:10.1016/j.atmosenv.2004.04.039, 2004a.
- Davis, D. D., Eisele, F., Chen, G., Crawford, J., Huey, G., Tanner, D., Slusher, D., Mauldin, L., Oncley, S., Lenschow, D., Semmer, S., Shetter, R., Lefer, B., Arimoto, R., Hogan, A., Grube, P., Lazzara, M., Bandy, A., Thornton, D., Berresheim, H., Bingemer, H., Hutterli, M., McConnell, J., Bales, R., Dibb, J., Buhr, M., Park, J., McMurry, P., Swanson, A., Meinardi, S., and Blake, D.: An overview of ISCAT 2000, *Atmos. Environ.*, 38, 5363–5373, doi:10.1016/j.atmosenv.2004.05.037, 2004b.
- Davis, D. D., Seelig, J., Huey, G., Crawford, J., Chen, G., Wang, Y. H., Buhr, M., Helmig, D., Neff, W., Blake, D., Arimoto, R., and Eisele, F.: A reassessment of Antarctic plateau reactive nitrogen based on ANTCI 2003 airborne and ground based measurements, *Atmos. Environ.*, 42, 2831–2848, doi:10.1016/j.atmosenv.2007.07.039, 2008.
- Eisele, F., Davis, D. D., Helmig, D., Oltmans, S. J., Neff, W., Huey, G., Tanner, D., Chen, G., Crawford, J., Arimoto, R., Buhr, M., Mauldin, L., Hutterli, M., Dibb, J., Blake, D., Brooks, S., Johnson, B., Roberts, J. M., Wang, Y., Tan, D., and Flocke, F.: Antarctic Tropospheric Chemistry Investigation (ANTCI) 2003 overview, *Atmos. Environ.*, 42, 2749–2761, 2008.
- France, J. L., King, M. D., Frey, M. M., Erbland, J., Picard, G., Preunkert, S., MacArthur, A., and Savarino, J.: Snow optical properties at Dome C (Concordia), Antarctica; implications for snow emissions and snow chemistry of reactive nitrogen, *Atmos. Chem. Phys.*, 11, 9787–9801, doi:10.5194/acp-11-9787-2011, 2011.
- Frey, M. M., Stewart, R. W., McConnell, J. R., and Bales, R. C.: Atmospheric hydroperoxides in West Antarctica: links to stratospheric ozone and atmospheric oxidation capacity, *J. Geophys. Res.*, 110, D23301, doi:10.1029/2005JD006110, 2005.
- Frey, M. M., Hutterli, M. A., Chen, G., Sjøstedt, S. J., Burkhardt, J. F., Friel, D. K., and Bales, R. C.: Contrasting atmospheric boundary layer chemistry of methylhydroperoxide (CH<sub>3</sub>OOH) and hydrogen peroxide (H<sub>2</sub>O<sub>2</sub>) above polar snow, *Atmos. Chem. Phys.*, 9, 3261–3276, doi:10.5194/acp-9-3261-2009, 2009a.
- Frey, M. M., Savarino, J., Morin, S., Erbland, J., and Martins, J. M. F.: Photolysis imprint in the nitrate stable isotope signal in snow and atmosphere of East Antarctica and implications for reactive nitrogen cycling, *Atmos. Chem. Phys.*, 9, 8681–8696, doi:10.5194/acp-9-8681-2009, 2009b.
- Genthon, C., Town, M. S., Six, D., Favier, V., Argentini, S., and Pellegrini, A.: Meteorological atmospheric boundary layer measurements and ECMWF analyses during summer at Dome C, Antarctica, *J. Geophys. Res.*, 115, D05104, doi:10.1029/2009JD012741, 2010.
- Grannas, A. M., Jones, A. E., Dibb, J., Ammann, M., Anastasio, C., Beine, H. J., Bergin, M., Bottenheim, J., Boxe, C. S., Carver, G., Chen, G., Crawford, J. H., Dominé, F., Frey, M. M., Guzmán, M. I., Heard, D. E., Helmig, D., Hoffmann, M. R., Honrath, R. E., Huey, L. G., Hutterli, M., Jacobi, H. W., Klán, P., Lefer, B., McConnell, J., Plane, J., Sander, R., Savarino, J., Shepson, P. B., Simpson, W. R., Sodeau, J. R., von Glasow, R., Weller, R., Wolff, E. W., and Zhu, T.: An overview of snow photochemistry: evidence, mechanisms and impacts, *Atmos. Chem. Phys.*, 7, 4329–4373, doi:10.5194/acp-7-4329-2007, 2007.
- Helmig, D., Boulter, J., David, D., Birks, J. W., Cullen, N. J., Steffen, K., Johnson, B. J., and Oltmans, S. J.: Ozone and meteorological boundary-layer conditions at Summit, Greenland, during 3–21 June 2000, *Atmos. Environ.*, 36, 2595–2608, 2002.
- Hoegstroem, U.: Non-dimensional wind and temperature profiles in the atmospheric surface layer: a re-evaluation, *Bound.-Lay. Meteorol.*, 42, 55–78, doi:10.1007/BF00119875, 1988.
- Honrath, R. E., Peterson, M. C., Dziobak, M. P., Dibb, J., Arseneault, M. A., and Green, S. A.: Release of NO<sub>x</sub> from sunlight-irradiated midlatitude snow, *Geophys. Res. Lett.*, 27, 2237–2240, 2000.
- Jacobson, M. Z.: *Fundamentals of Atmospheric Modeling*, Cambridge University Press, Cambridge, UK, 656 pp., 1999.

- Jones, A. E., Wolff, E. W., Salmon, R. A., Bauguitte, S. J.-B., Roscoe, H. K., Anderson, P. S., Ames, D., Clemittshaw, K. C., Fleming, Z. L., Bloss, W. J., Heard, D. E., Lee, J. D., Read, K. A., Hamer, P., Shallcross, D. E., Jackson, A. V., Walker, S. L., Lewis, A. C., Mills, G. P., Plane, J. M. C., Saiz-Lopez, A., Sturges, W. T., and Worton, D. R.: Chemistry of the Antarctic Boundary Layer and the Interface with Snow: an overview of the CHABLIS campaign, *Atmos. Chem. Phys.*, 8, 3789–3803, doi:10.5194/acp-8-3789-2008, 2008.
- Jones, A. E., Wolff, E. W., Ames, D., Bauguitte, S. J.-B., Clemittshaw, K. C., Fleming, Z., Mills, G. P., Saiz-Lopez, A., Salmon, R. A., Sturges, W. T., and Worton, D. R.: The multi-seasonal NO<sub>y</sub> budget in coastal Antarctica and its link with surface snow and ice core nitrate: results from the CHABLIS campaign, *Atmos. Chem. Phys.*, 11, 9271–9285, doi:10.5194/acp-11-9271-2011, 2011.
- Kaimal, J. and Finnigan, J. J.: *Atmospheric Boundary Layer Flows*, Oxford University Press, Oxford, UK, 289 pp., 1994.
- Kerbrat, M., Legrand, M., Preunkert, S., Gallée, H., and Kleffmann, J.: Nitrous acid at Concordia (inland site) and Dumont d'Urville (coastal site), East Antarctica, *J. Geophys. Res.*, 117, D08303, doi:10.1029/2011JD017149, 2012.
- King, J. C. and Anderson, P. S.: Heat and water vapor fluxes and scalar roughness lengths over an Antarctic ice shelf, *Bound.-Lay. Meteorol.*, 69, 101–121, 1994.
- King, J. C., Argentini, S. A., and Anderson, P. S.: Contrasts between the summertime surface energy balance and boundary layer structure at Dome C and Halley stations, Antarctica, *J. Geophys. Res.*, 111, D02105, doi:10.1029/2005JD006130, 2006.
- Kuhn, H., Lettau, H., and Riordan, A.: Stability-related wind spiraling in the lowest 32 meters, in: *Meteorological Studies at Plateau Station, Antarctica*, edited by: Businger, J., vol. 25 of *Antarct. Res. Ser.*, AGU, Washington D.C., 93–111, 1977.
- Lee-Taylor, J. and Madronich, S.: Calculation of actinic fluxes with a coupled atmosphere-snow radiative transfer model, *J. Geophys. Res.*, 107, D244796, doi:10.1029/2002JD002084, 2002.
- Legrand, M., Preunkert, S., Jourdain, B., Gallée, H., Goutail, F., Weller, R., and Savarino, J.: Year-round record of surface ozone at coastal (Dumont d'Urville) and inland (Concordia) sites in East Antarctica, *J. Geophys. Res.*, 114, D20306, doi:10.1029/2008JD011667, 2009.
- Leighton, P. A.: *Photochemistry of air pollution*, Academic Press, New York, 1961.
- Lenschow, D. H.: Micrometeorological techniques for measuring biosphere-atmosphere trace gas exchange, in: *Biogenic Trace Gases: Measuring Emissions from Soil and Water*, edited by: Matson, P. A. and Harriss, R. C., Blackwell Science, London, 126–163, 1995.
- Liao, W., Case, A. T., Mastromarino, J., Tan, D., and Dibb, J. E.: Observations of HONO by laser-induced fluorescence at the South Pole during ANTCI 2003, *Geophys. Res. Lett.*, 33, L09810, doi:10.1029/2005GL025470, 2006.
- Maindonald, J. and Braun, J.: *Data analysis and graphics using R – an example-based approach*, Cambridge Series in Statistical and Probabilistic Mathematics, Cambridge University Press, Cambridge, UK, , 384 pp., 2003.
- Neff, W., Helmig, D., Grachev, A., and Davis, D.: A study of boundary layer behavior associated with high NO concentrations at the South Pole using a minisodar, tethered balloons and sonic anemometer, *Atmos. Environ.*, 42, 2762–2779, doi:10.1016/j.atmosenv.2007.01.033, 2008.
- Oncley, S. P., Buhr, M., Lenschow, D. H., Davis, D., and Semmer, S. R.: Observations of summertime NO fluxes and boundary-layer height at the South Pole during ISCAT 2000 using scalar similarity, *Atmos. Environ.*, 38, 5389–5398, doi:10.1016/j.atmosenv.2004.05.053, 2004.
- Pollard, R., Rhines, P. B., and Thompson, R.: The deepening of the wind-mixed layer, *Geophys. Fluid Dyn.*, 3, 381–404, 1973.
- Ridley, B., Walega, J., Montzka, D., Grahek, F., Atlas, E., Flocke, F., Stroud, V., Deary, J., Gallant, A., Boudries, H., Bottenheim, J., Anlauf, K., Worthy, D., Sumner, A., Splawn, B., and Shepson, P.: Is the Arctic surface layer a source and sink of NO<sub>x</sub> in winter/spring, *J. Atmos. Chem.*, 36, 1–22, 2000.
- Röthlisberger, R., Hutterli, M. A., Wolff, E. W., Mulvaney, R., Fischer, H., Bigler, M., Goto-Azuma, K., Hansson, M. E., Ruth, U., Siggaard-Andersen, M. L., and Steffensen, J. P.: Nitrate in Greenland and Antarctic ice cores: a detailed description of post-depositional processes, *Ann. Glaciol.*, 35, 209–216, 2002.
- Ryerson, T. B., Williams, E. J., and Fehsenfeld, F. C.: An efficient photolysis system for fast-response NO<sub>2</sub> measurements, *J. Geophys. Res.*, 105, 26447–26461, 2000.
- Sander, R. and Bottenheim, J.: A compilation of tropospheric measurements of gas-phase and aerosol chemistry in polar regions, *Earth Sys. Sci. Data*, 4, 215–282, doi:10.5194/essd-4-215-2012, 2012.
- Sander, S. P., Friedl, R. R., Golden, D. M., Kurylo, M. J., Moortgat, G. K., Wine, P. H., Ravishankara, A., Kolb, C. E., Molina, M., Finlayson-Pitts, B. J., Huie, R. E., and Orkin, V. L.: *Chemical Kinetics and Photochemical Data for Use in Atmospheric Studies*, Tech. Rep. Eval. No. 15, Jet Propulsion Laboratory, Pasadena, California, USA, 2006.
- Sjostedt, S. J., Huey, L. G., Tanner, D. J., Peischl, J., Chen, G., Dibb, J. E., Lefer, B., Hutterli, M. A., Beyersdorf, A. J., Blake, N. J., Blake, D. R., Sueper, D., Ryerson, T., Burkhardt, J., and Stohl, A.: Observations of hydroxyl and the sum of peroxy radicals at Summit, Greenland during summer 2003, *Atmos. Environ.*, 41, 5122–5137, 2007.
- Slusher, D. L., Neff, W. D., Kim, S., Huey, L. G., Wang, Y., Zeng, T., Tanner, D. J., Blake, D. R., Beyersdorf, A., Lefer, B. L., Crawford, J. H., Eisele, F. L., Mauldin, R. L., Kosciuch, E., Buhr, M. P., Wallace, H. W., and Davis, D. D.: Atmospheric chemistry results from the ANTCI 2005 Antarctic plateau airborne study, *J. Geophys. Res.*, 115, D07304, doi:10.1029/2009JD012605, 2010.
- Stull, R. B.: *An Introduction to Boundary Layer Meteorology*, Kluwer Academic Publishers, Dordrecht, the Netherlands, 670 pp., 1988.
- Thomas, J. L., Stutz, J., Lefer, B., Huey, L. G., Toyota, K., Dibb, J. E., and von Glasow, R.: Modeling chemistry in and above snow at Summit, Greenland – Part 1: Model description and results, *Atmos. Chem. Phys.*, 11, 4899–4914, doi:10.5194/acp-11-4899-2011, 2011.
- Van Dijk, A., Moen, A., and De Bruin, H.: *The principles of surface flux physics: theory, practice and description of the ECPACK library*, Internal Report 2004/1, Meteorology and Air Quality Group, Wageningen University, Wageningen, the Netherlands, 2006.

Zhu, C. Z., Xiang, B., Chu, L. T., and Zhu, L.: 308 nm photolysis of nitric acid in the gas phase, on aluminum surfaces, and on ice films, *J. Phys. Chem. A*, 114, 2561–2568, doi:10.1021/jp909867a, 2010.

Zilitinkevitch, S., Baklanov, A., Rost, J., Smedman, A., Lykosov, V., and Calanca, P.: Calculation of the height of the stable boundary layer in practical applications, *Bound.-Lay. Meteorol.*, 105, 389–409, 2002.